

## A GODUNOV-TYPE SCHEME AND A RELAXATION SCHEME FOR SECOND-ORDER TURBULENCE-MOMENT MODELS

NADJIB BENNOURA BOUCHIBA, MARTIN FERRAND AND JEAN-MARC HÉRARD\*

**Abstract.** A Godunov-type scheme and a relaxation scheme are presented to approximate the solutions of the convective subsystem arising from the transport equations of a class of second-order turbulence-moment models in the framework of incompressible flows. An analytical representation is proposed for the case of the occurrence of a non-turbulent region. Numerical tests of the two schemes and a comparison with a Rusanov scheme complete the paper.

**Mathematics Subject Classification.** 35Q35, 76-10, 76M12, 35Lxx.

Received November 18, 2024. Accepted July 29, 2025.

### 1. INTRODUCTION

Turbulence is a fundamental phenomenon in fluid dynamics, and its modelling is of prime importance, *e.g.*, for thermallydraulics, fire modelling, or in atmospheric flow simulations. A traditional way of modelling turbulent flows is to consider Reynolds-averaged Navier-Stokes equations, but necessitates closure laws for the fluid velocity covariance, called the Reynolds stress tensor. The Reynolds stress tensor in the momentum equation, whose divergence is a convection term, is commonly replaced by an eddy viscosity model, which gives an additional diffusive contribution. This type of closure has limitations in accurately representing turbulence for a wide range of flows (*e.g.*, point source dispersion, rotating flows, etc.) but are still commonly used due to their numerical robustness. To remedy this, transport equations of second-order turbulence-moments may be considered, which provide a more accurate description of turbulence by modelling the transport of the Reynolds stress tensor, taking into account convection, diffusion, and source terms. This type of approach has also been recently used to tackle shallow-water shear flows (see [4, 20, 31, 44]).

The equations describing mass and momentum conservation as well as the transport of the Reynolds stress tensor  $\mathbf{R} = \bar{\mathbf{u}}' \otimes \bar{\mathbf{u}}'$  for an incompressible flow write:

$$\begin{cases} \operatorname{div} \bar{\mathbf{u}} = 0, \\ \partial_t \bar{\mathbf{u}} + (\bar{\mathbf{u}} \cdot \nabla) \bar{\mathbf{u}} + \operatorname{div} \mathbf{R} = -\frac{1}{\rho_0} \nabla \bar{p} + \operatorname{div} [\nu_0 (\nabla \bar{\mathbf{u}})], \\ \partial_t \mathbf{R} + (\bar{\mathbf{u}} \cdot \nabla) \mathbf{R} + (\nabla \bar{\mathbf{u}} \cdot \mathbf{R} + \mathbf{R} \cdot \nabla \bar{\mathbf{u}}^T) = \Psi(\mathbf{Y}) + \operatorname{div} [(\nu_0 + \gamma_t(\mathbf{Y})) \nabla \mathbf{R}], \end{cases} \quad (1.1)$$

---

*Keywords and phrases.* Second-order turbulence-moment models, incompressible flows, Godunov scheme, relaxation scheme, laminar/turbulent flows, Riemann problem.

CEREA, EDF R&D, École des Ponts, Île de France, France.

\*Corresponding author: [herard.aubry@wanadoo.fr](mailto:herard.aubry@wanadoo.fr); [jean-marc.herard@edf.fr](mailto:jean-marc.herard@edf.fr)

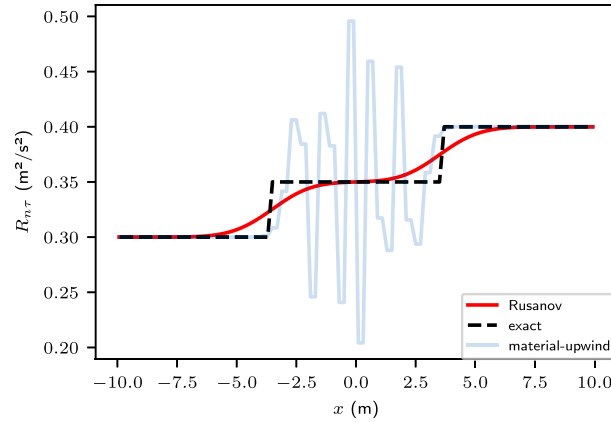


FIGURE 1. Illustration of instabilities occurring with material-upwind scheme, reproduced from [17].

with suitable initial and boundary conditions and we write the variable as  $\mathbf{Y} = (\bar{\mathbf{u}}, \bar{p}, \mathbf{R})^T$ ,  $\bar{\mathbf{u}}$ ,  $\bar{p}$  being, respectively, the Reynolds averaged velocity and pressure. Here, positive parameters  $\rho_0$  and  $\nu_0$  are, respectively, the density and the kinematic viscosity of the fluid under consideration. The diffusivity  $\gamma_t(\mathbf{Y}) \geq 0$  and the correlation  $\Psi(\mathbf{Y})$  are given by a closure relation ( $\Psi$  is such that  $\Psi(\bar{\mathbf{u}}, \bar{p}, \mathbf{R} = \mathbf{0}) = \mathbf{0}$ ), as the model proposed by Rotta [37] and recalled in [34], Section 11.3.1, which can be recast in the form:

$$\Psi(\mathbf{Y}) = \frac{C_R - 1}{T} \frac{\text{trace}(\mathbf{R})}{3} \mathbf{1} - \frac{C_R}{T} \mathbf{R}, \quad (1.2)$$

where  $T$  is the integral turbulence timescale. Most turbulent models take the constant  $C_R$  to be greater than 1 to ensure a return to isotropy (see [37]). Whatever the value of  $C_R$ , model (1.2) contributes to the decrease in turbulent kinetic energy ( $\text{trace}(\mathbf{R})/2$ ) and to the decrease of the total energy  $\mathcal{E} = \frac{1}{2}(\bar{\mathbf{u}} \cdot \bar{\mathbf{u}} + \text{trace}(\mathbf{R}))$ . This model is similar to the “ideal” turbulence model proposed in [46].

The Reynolds stress tensor  $\mathbf{R}$  is a covariance matrix and is symmetric positive and half-definite. This particular property of the Reynolds stress tensor, which must remain satisfied over time, is called the realisability property (see, *e.g.*, [15, 23, 28, 34, 40]). Formally, when  $\mathbf{R} = \mathbf{0}$ , the Navier–Stokes equations for incompressible laminar flow are retrieved.

However, discretising the second-order turbulence-moment transport equations in space and time in a stable manner represents a challenge. In fact, most schemes used in CFD codes feature a material-upwinding of convective terms relying on the sole eigenvalue  $\lambda = \bar{u}$ ,  $\bar{u}$  being the local velocity, associated with the operator  $\partial_t(\cdot) + (\bar{\mathbf{u}} \cdot \nabla)(\cdot)$ . The other convective terms, namely  $\text{div} \mathbf{R}$  and  $\nabla \bar{\mathbf{u}} \cdot \mathbf{R} + \mathbf{R} \cdot \nabla \bar{\mathbf{u}}^T$ , are usually discretised using centred schemes. This treatment is not adequate due to the arising of other waves in the system, as presented in [17, 24], and recalled in Section 2, Property 2.1. This material-upwinding indeed gives rise to numerical instabilities as highlighted in [6] (respectively, in [36]) in the compressible (respectively, incompressible) framework. This has been illustrated in [17], Figure 3, page 351 and reproduced in Figure 1.

In order to eliminate oscillations arising with material-upwinding, approximate solutions of (1.1) are computed using the algorithm detailed in the sequel. Two steps are introduced to go from the state at time  $t^N$  to time  $t^{N+1}$ :

- **Step 1:** Compute the – explicit – approximate solution  $(\bar{\mathbf{u}}^\#, \mathbf{R}^\#)$  of the convective (and hyperbolic, see [24]) subsystem, corresponding to the left-hand-side of second and third equations in (1.1), considering initial

condition  $(\bar{\mathbf{u}}^N, \mathbf{R}^N)$  and suitable boundary conditions:

$$\begin{cases} \frac{\bar{\mathbf{u}}^\# - \bar{\mathbf{u}}^N}{\delta t} + ((\bar{\mathbf{u}} \cdot \nabla)\bar{\mathbf{u}} + \mathbf{div} \mathbf{R})^N = 0, \\ \frac{\mathbf{R}^\# - \mathbf{R}^N}{\delta t} + ((\bar{\mathbf{u}} \cdot \nabla)\mathbf{R} + (\nabla\bar{\mathbf{u}} \cdot \mathbf{R} + \mathbf{R} \cdot \nabla\bar{\mathbf{u}}^T))^N = 0. \end{cases} \tag{1.3}$$

– **Step 2:** Update  $\mathbf{Y}^{N+1}$ , starting from  $(\bar{\mathbf{u}}^\#, \mathbf{R}^\#)$ , looking for approximate solutions of:

$$\begin{cases} \mathbf{div} \bar{\mathbf{u}}^{N+1} = 0, \\ \frac{\bar{\mathbf{u}}^{N+1} - \bar{\mathbf{u}}^\#}{\delta t} + \left( \frac{1}{\rho_0} \nabla \bar{p} - \mathbf{div} [\nu_0(\nabla\bar{\mathbf{u}})] \right)^{N+1} = 0, \\ \frac{\mathbf{R}^{N+1} - \mathbf{R}^\#}{\delta t} - (\Psi(\mathbf{Y}) + \mathbf{div}((\nu_0 + \gamma_t(\mathbf{Y}))\nabla\mathbf{R}))^{N+1} = 0, \end{cases} \tag{1.4}$$

supplemented by suitable boundary conditions.

Within step 2, the first two equations in system (1.4) represent a Stokes-like problem for an unsteady configuration (see [11, 43]). They are decoupled from the third equation in (1.4), which only involves source terms and diffusive contributions with respect to the Reynolds stress tensor.

The main objective in the present paper is to define relevant *numerical schemes in order to account for the convective part of second-order turbulence-moment transport equations* (1.3), hence computing an approximate solution  $(\bar{\mathbf{u}}^\#, \mathbf{R}^\#)$ .

The main properties of the continuous convective subsystem associated with (1.3) which have been investigated in [17, 24] are recalled in Section 2. Then a special focus on the non-turbulent region is given in Section 3. A Godunov-type scheme based on the solution of the Riemann problem is presented first in Section 4. The construction of a relaxation scheme based on the leading works of Chen *et al.* [10], Jin and Xin [25], Suliciu [42], Natalini [30], Bouchut [5], Chalons and Coulombel [9], Coquel *et al.* [12], allowing accurate results while reducing CPU costs, is carried out in Section 5. Section 6 provides some numerical results, with a measure of the error in  $L^1$  norm, while focusing on Riemann problems.

## 2. A SUMMARY OF THE PROPERTIES OF THE CONVECTIVE SYSTEM IN STRICTLY TURBULENT CASES

The two-dimensional framework is considered in the following for the sake of conciseness but this can be extended to the tridimensional framework. We recall that the convective subsystem:

$$\begin{cases} \partial_t \bar{\mathbf{u}} + (\bar{\mathbf{u}} \cdot \nabla)\bar{\mathbf{u}} + \mathbf{div} \mathbf{R} = 0, \\ \partial_t \mathbf{R} + (\bar{\mathbf{u}} \cdot \nabla)\mathbf{R} + (\nabla\bar{\mathbf{u}} \cdot \mathbf{R} + \mathbf{R} \cdot \nabla\bar{\mathbf{u}}^T) = 0, \end{cases} \tag{2.1}$$

is hyperbolic (see [24], Prop. IV).

Therefore, a classical finite-volume approach to define approximate solutions is to build one-dimensional Riemann solvers at the cell interfaces (of unit normal denoted by  $\mathbf{e}_n$ ), using the rotation invariance of the convective subsystem (2.1), and disposing of the transverse derivatives to the face (see, *e.g.*, [45], Chap. 16.4). The transverse direction to the face is denoted by  $\mathbf{e}_\tau$ . In the following, system (2.1) is rewritten in the reference frame  $(\mathbf{e}_n, \mathbf{e}_\tau)$ , while eliminating transverse derivatives:

$$\begin{cases} \partial_t u_n + u_n \partial_n u_n + \partial_n R_{nn} = 0, \\ \partial_t R_{nn} + u_n \partial_n R_{nn} + 2R_{nn} \partial_n u_n = 0, \\ \partial_t u_\tau + u_n \partial_n u_\tau + \partial_n R_{n\tau} = 0, \\ \partial_t R_{n\tau} + u_n \partial_n R_{n\tau} + R_{nn} \partial_n u_\tau + R_{n\tau} \partial_n u_n = 0, \\ \partial_t R_{\tau\tau} + u_n \partial_n R_{\tau\tau} + 2R_{n\tau} \partial_n u_\tau = 0, \end{cases} \tag{2.2}$$

where:

$$u_n = \bar{\mathbf{u}} \cdot \mathbf{e}_n, \tag{2.3a}$$

$$u_\tau = \bar{\mathbf{u}} \cdot \mathbf{e}_\tau, \tag{2.3b}$$

$$R_{nn} = \mathbf{e}_n \cdot \mathbf{R} \cdot \mathbf{e}_n, \tag{2.3c}$$

$$R_{\tau\tau} = \mathbf{e}_\tau \cdot \mathbf{R} \cdot \mathbf{e}_\tau, \tag{2.3d}$$

$$R_{n\tau} = \mathbf{e}_n \cdot \mathbf{R} \cdot \mathbf{e}_\tau = R_{\tau n}. \tag{2.3e}$$

We also note  $x_n = \mathbf{x} \cdot \mathbf{e}_n$  and, in order to simplify the notations, we will write  $x$  instead of  $x_n$  in the sequel. We define the main unknown  $\mathbf{w}$  as:

$$\mathbf{w} = (u_n, R_{nn}, u_\tau, R_{n\tau}, R_{\tau\tau}). \tag{2.4}$$

We now recall the main properties of (2.2) (see [17, 24]).

**Property 2.1** (Hyperbolicity of system (2.2)). For  $R_{nn} > 0$ , the convective matrix arising from (2.2) has five real eigenvalues:

$$\lambda_1 = u_n - \sqrt{2R_{nn}}, \quad \lambda_2 = u_n - \sqrt{R_{nn}}, \quad \lambda_3 = u_n, \quad \lambda_4 = u_n + \sqrt{R_{nn}}, \quad \lambda_5 = u_n + \sqrt{2R_{nn}}. \tag{2.5}$$

We note that associated right eigenvectors span  $\mathbb{R}^5$ .

One can observe that the realisability of the Reynolds stress tensor guarantees the hyperbolicity of the convective subsystem.

**Property 2.2** (Characteristic fields and Riemann invariants).

- Fields associated with  $\lambda_1$  and  $\lambda_5$  are genuinely non linear (GNL) while those associated with  $\lambda_2, \lambda_3$  and  $\lambda_4$  are linearly degenerate (LD). The intermediate states between these fields are depicted in Figure 2.
- The list of Riemann invariants through the  $k$ -wave is denoted by  $I_R^k$ . Riemann invariants within each field are recalled below:

$$I_R^1 = \left\{ u_n + \sqrt{2R_{nn}}, \frac{R_{n\tau}}{R_{nn}}, R_{\tau\tau} - \frac{R_{n\tau}^2}{R_{nn}}, u_\tau + R_{n\tau} \sqrt{\frac{2}{R_{nn}}} \right\}, \tag{2.6a}$$

$$I_R^2 = \left\{ u_n, R_{nn}, u_\tau + \frac{R_{n\tau}}{\sqrt{R_{nn}}}, R_{\tau\tau}R_{nn} - R_{n\tau}^2 \right\}, \tag{2.6b}$$

$$I_R^3 = \left\{ u_n, R_{nn}, u_\tau, R_{n\tau} \right\}, \tag{2.6c}$$

$$I_R^4 = \left\{ u_n, R_{nn}, u_\tau - \frac{R_{n\tau}}{\sqrt{R_{nn}}}, R_{\tau\tau}R_{nn} - R_{n\tau}^2 \right\}, \tag{2.6d}$$

$$I_R^5 = \left\{ u_n - \sqrt{2R_{nn}}, \frac{R_{n\tau}}{R_{nn}}, R_{\tau\tau} - \frac{R_{n\tau}^2}{R_{nn}}, u_\tau - R_{n\tau} \sqrt{\frac{2}{R_{nn}}} \right\}. \tag{2.6e}$$

**Assumption 2.1** (Approximate shock relations). *Since system (2.2) does not have a conservative form, we consider the following approximate shock relations, as assumed in [24] and [17]:*

$$\begin{cases} \sigma[u_n]_l^r = \widehat{u_n}^{l|r} [u_n]_l^r + [R_{nn}]_l^r, \\ \sigma[u_\tau]_l^r = \widehat{u_\tau}^{l|r} [u_\tau]_l^r + [R_{n\tau}]_l^r, \\ \sigma[R_{nn}]_l^r = 2\widehat{R_{nn}}^{l|r} [u_n]_l^r + \widehat{u_n}^{l|r} [R_{nn}]_l^r, \\ \sigma[R_{n\tau}]_l^r = \widehat{R_{n\tau}}^{l|r} [u_n]_l^r + \widehat{R_{nn}}^{l|r} [u_\tau]_l^r + \widehat{u_n}^{l|r} [R_{n\tau}]_l^r, \\ \sigma[R_{\tau\tau}]_l^r = 2\widehat{R_{\tau\tau}}^{l|r} [u_\tau]_l^r + \widehat{u_\tau}^{l|r} [R_{\tau\tau}]_l^r, \end{cases} \tag{2.7}$$

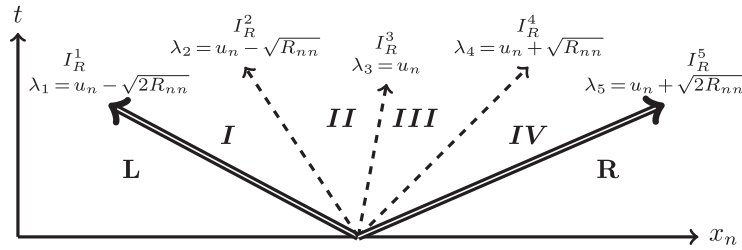


FIGURE 2. Convective subsystem (2.2) intermediate states.

where we recall  $[\phi]_l^r := \phi_r - \phi_l$ ,  $\widehat{\phi}^{lr} := \frac{1}{2}(\phi_r + \phi_l)$ ,  $\sigma$  is the speed of the discontinuity. These are only valid for weak shocks (see [13, 26]), and are obtained using a linear path with respect to the variable  $\mathbf{w}$  in (2.4).

Approximate relations (2.7) can also be obtained from transport equations written in pseudo-conservative variables  $\mathbf{R} + \bar{\mathbf{u}} \otimes \bar{\mathbf{u}}$  instead of  $\mathbf{R}$ , as explained in [24], page 18 and Appendix 4. This choice also preserves the realisability of intermediate states as presented in Remark 4.1.

**Remark 2.1.**

- Note that a smooth solution  $R_{nn}$  of the second equation of (2.2) should remain positive with adequate initial and boundary conditions, and assuming  $\partial_n u_n$  bounded (see [27]).
- Moreover, the quantity  $\delta_2 := R_{nn}R_{\tau\tau} - R_{n\tau}^2$  satisfies the following evolution equation (see [17]):

$$\partial_t \delta_2 + u_n \partial_n \delta_2 + 2\delta_2 \partial_n u_n = 0, \tag{2.8}$$

again allowing us to conclude that  $\delta_2(x, t) \geq 0$  (still assuming positive initial and boundary conditions, and  $\partial_n u_n$  bounded).

The following result holds (see [17, 24] for details):

**Property 2.3** (Solution of the one-dimensional Riemann problem associated to (2.2)). Considering the shock relations (2.7), the existence and uniqueness of the strictly realisable self-similar solution (that is with  $R_{nn} > 0$  and  $R_{nn}R_{\tau\tau} - R_{n\tau}^2 > 0$ ) of the one-dimensional Riemann problem associated with (2.2), for given strictly realisable left state  $\mathbf{w}^L$  and strictly realisable right state  $\mathbf{w}^R$ , is fulfilled when condition:

$$u_n^R - u_n^L < \sqrt{2R_{nn}^R} + \sqrt{2R_{nn}^L}, \tag{2.9}$$

is satisfied.

The calculation of intermediate states, when this condition is satisfied, is given in [17]. It will be used in Section 4 when implementing the Godunov-type scheme.

### 3. EXTENSION OF THE SOLUTION IN THE EMERGENCE OF A NON-TURBULENT STATE

When relation (2.9) is violated, null values of  $R_{nn}$  may arise. In this section, we investigate a one-dimensional Riemann problem with the following initial realisable conditions:

$$\mathbf{w}(x < 0, t = 0) = \mathbf{w}^L, \tag{3.1}$$

$$\mathbf{w}(x > 0, t = 0) = \mathbf{w}^R, \tag{3.2}$$

such that (2.9) no longer holds, hence:

$$u_n^R - u_n^L \geq \sqrt{2R_{nn}^R} + \sqrt{2R_{nn}^L}. \tag{3.3}$$

In the limit case  $\sqrt{2R_{nn}^R} + \sqrt{2R_{nn}^L} - (u_n^R - u_n^L) \rightarrow 0^+$ , the solution is composed of a 1-rarefaction wave and a 5-rarefaction wave that meet. Therefore, when (3.3) holds, we look for a solution composed of a 1-rarefaction wave and a 5-rarefaction wave, separated by a non-turbulent region where  $R_{nn} = 0$ , as depicted in Figure 3 (see [16] for the counterpart in the gas dynamics vacuum case).

In what follows, for a function  $\phi(x, t)$ , we denote by  $\tilde{\phi}(\frac{x}{t})$  the associated function of the variable  $\frac{x}{t}$ .

### 3.1. Self-similar solution in the turbulent regions

Let us first describe the self-similar solution outside the non-turbulent region:

- It is the left state  $w^L$  when  $\frac{x}{t} < \lambda_1(w^L) = u_n^L - \sqrt{2R_{nn}^L}$  and the right state  $w^R$  when  $\frac{x}{t} > \lambda_5(w^R) = u_n^R + \sqrt{2R_{nn}^R}$ , thus:

$$w(x, t) = \tilde{w}\left(\frac{x}{t}\right) = w^L \quad \text{for} \quad \frac{x}{t} < \lambda_1(w^L), \tag{3.4}$$

and:

$$w(x, t) = \tilde{w}\left(\frac{x}{t}\right) = w^R \quad \text{for} \quad \frac{x}{t} > \lambda_5(w^R). \tag{3.5}$$

- The left state  $w^L$  is connected to the non-turbulent area (where  $R_{nn} = 0$ ) through a 1-rarefaction wave for:

$$\lambda_1(w^L) < \frac{x}{t} < u_n^- = \lambda_1(w^-), \tag{3.6}$$

where  $u_n^-$  corresponds to the limit value in the 1-rarefaction wave associated with  $R_{nn}^- = 0$ , thus:

$$u_n^- = u_n^- + \sqrt{2R_{nn}^-} = u_n^L + \sqrt{2R_{nn}^L}, \tag{3.7}$$

according to the first Riemann invariant of the 1-wave  $u_n + \sqrt{2R_{nn}}$  given in (2.6a).

The variable  $\tilde{w}(\frac{x}{t})$  inside the 1-rarefaction wave (3.6), that is for  $\frac{x}{t}$  such as  $\lambda_1(w^L) = u_n^L - \sqrt{2R_{nn}^L} < \frac{x}{t} < u_n^- = \lambda_1(w^-)$ , is calculated according to the Riemann invariants (2.6a) of the 1-wave and the relation  $\lambda_1(\tilde{w}) = \frac{x}{t}$ :

$$\left\{ \begin{aligned} \tilde{u}_n\left(\frac{x}{t}\right) &= \frac{1}{2}\left(u_n^L + \sqrt{2R_{nn}^L} + \frac{x}{t}\right), \\ \tilde{R}_{nn}\left(\frac{x}{t}\right) &= \frac{1}{8}\left(u_n^L + \sqrt{2R_{nn}^L} - \frac{x}{t}\right)^2, \\ \tilde{R}_{n\tau}\left(\frac{x}{t}\right) &= \frac{R_{n\tau}^L}{R_{nn}^L} \tilde{R}_{nn}\left(\frac{x}{t}\right), \\ \tilde{u}_\tau\left(\frac{x}{t}\right) &= u_\tau^L + R_{n\tau}^L \sqrt{\frac{2}{R_{nn}^L}} - \tilde{R}_{n\tau}\left(\frac{x}{t}\right) \sqrt{\frac{2}{\tilde{R}_{nn}\left(\frac{x}{t}\right)}}, \\ \tilde{R}_{\tau\tau}\left(\frac{x}{t}\right) &= R_{\tau\tau}^L - \frac{(R_{n\tau}^L)^2}{R_{nn}^L} + \frac{(\tilde{R}_{n\tau}\left(\frac{x}{t}\right))^2}{\tilde{R}_{nn}\left(\frac{x}{t}\right)}. \end{aligned} \right. \tag{3.8}$$

Note that by isolating the Riemann 1- invariant  $\frac{R_{n\tau}}{R_{nn}}$ , the latter two components may be rewritten as:

$$\left\{ \begin{aligned} \tilde{u}_\tau\left(\frac{x}{t}\right) &= u_\tau^L + \frac{R_{n\tau}^L}{R_{nn}^L} \left( \sqrt{2R_{nn}^L} - \sqrt{2\tilde{R}_{nn}\left(\frac{x}{t}\right)} \right), \\ \tilde{R}_{\tau\tau}\left(\frac{x}{t}\right) &= R_{\tau\tau}^L - \left( \frac{R_{n\tau}^L}{R_{nn}^L} \right)^2 \left( R_{nn}^L - \tilde{R}_{nn}\left(\frac{x}{t}\right) \right), \end{aligned} \right. \tag{3.9}$$

which will be used in the sequel.

– In a similar way, the right state  $\mathbf{w}^R$  is connected to the non-turbulent region where  $R_{nn}^+ = 0$  through a 5-rarefaction wave, for  $\frac{x}{t}$  such as  $\lambda_5(\mathbf{w}^+) = u_n^+ < \frac{x}{t} < \lambda_5(\mathbf{w}^R)$ , defining:

$$u_n^+ = u_n^+ - \sqrt{2R_{nn}^+} = u_n^R - \sqrt{2R_{nn}^R}, \tag{3.10}$$

It is crucial to note that:

$$u_n^+ = u_n^R - \sqrt{2R_{nn}^R} > u_n^L + \sqrt{2R_{nn}^L} = u_n^-, \tag{3.11}$$

because of the violation of the condition (2.9).

Hence, the variable  $\tilde{\mathbf{w}}(\frac{x}{t})$  inside the 5-rarefaction wave, for  $\lambda_5(\mathbf{w}^+) < \frac{x}{t} < \lambda_5(\mathbf{w}^R)$ , writes:

$$\left\{ \begin{aligned} \tilde{u}_n(\frac{x}{t}) &= \frac{1}{2} \left( u_n^R - \sqrt{2R_{nn}^R} + \frac{x}{t} \right), \\ \tilde{R}_{nn}(\frac{x}{t}) &= \frac{1}{8} \left( u_n^R - \sqrt{2R_{nn}^R} - \frac{x}{t} \right)^2, \\ \tilde{R}_{n\tau}(\frac{x}{t}) &= \frac{R_{n\tau}^R}{R_{nn}^R} \tilde{R}_{nn}(\frac{x}{t}), \\ \tilde{u}_\tau(\frac{x}{t}) &= u_\tau^R - R_{n\tau}^R \sqrt{\frac{2}{R_{nn}^R}} + \tilde{R}_{n\tau}(\frac{x}{t}) \sqrt{\frac{2}{\tilde{R}_{nn}(\frac{x}{t})}}, \\ \tilde{R}_{\tau\tau}(\frac{x}{t}) &= R_{\tau\tau}^R - \frac{(R_{n\tau}^R)^2}{R_{nn}^R} + \frac{(\tilde{R}_{n\tau}(\frac{x}{t}))^2}{\tilde{R}_{nn}(\frac{x}{t})}. \end{aligned} \right. \tag{3.12}$$

The latter components rewrite:

$$\left\{ \begin{aligned} \tilde{u}_\tau(\frac{x}{t}) &= u_\tau^R - \frac{R_{n\tau}^R}{R_{nn}^R} \left( \sqrt{2R_{nn}^R} - \sqrt{2\tilde{R}_{nn}(\frac{x}{t})} \right), \\ \tilde{R}_{\tau\tau}(\frac{x}{t}) &= R_{\tau\tau}^R - \left( \frac{R_{n\tau}^R}{R_{nn}^R} \right)^2 \left( R_{nn}^R - \tilde{R}_{nn}(\frac{x}{t}) \right). \end{aligned} \right. \tag{3.13}$$

Let us now define the so-called edge states  $\mathbf{w}^-$  and  $\mathbf{w}^+$  corresponding respectively to the right edge of the 1-rarefaction wave (left state of the non-turbulent region) and the left edge of the 5-rarefaction wave (right state of the non-turbulent region):

$$\left\{ \begin{aligned} u_n^- &= u_n^L + \sqrt{2R_{nn}^L}, \\ R_{nn}^- &= 0, \\ R_{n\tau}^- &= 0, \\ u_\tau^- &= u_\tau^L + R_{n\tau}^L \sqrt{\frac{2}{R_{nn}^L}}, \\ R_{\tau\tau}^- &= R_{\tau\tau}^L - \frac{(R_{n\tau}^L)^2}{R_{nn}^L}, \end{aligned} \right. \tag{3.14}$$

$$\left\{ \begin{aligned} u_n^+ &= u_n^R - \sqrt{2R_{nn}^R}, \\ R_{nn}^+ &= 0, \\ R_{n\tau}^+ &= 0, \\ u_\tau^+ &= u_\tau^R - R_{n\tau}^R \sqrt{\frac{2}{R_{nn}^R}}, \\ R_{\tau\tau}^+ &= R_{\tau\tau}^R - \frac{(R_{n\tau}^R)^2}{R_{nn}^R}. \end{aligned} \right. \tag{3.15}$$

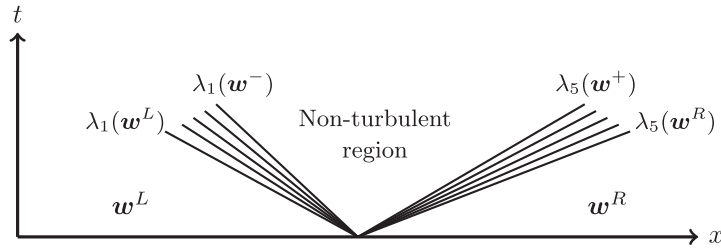


FIGURE 3. Non-turbulent region occurrence.

### 3.2. Self-similar solution in the non-turbulent region

Inside the non-turbulent region for  $\lambda_1(\mathbf{w}^-) = u_n^- < \frac{x}{t} < \lambda_5(\mathbf{w}^+) = u_n^+$ , we have:

$$\tilde{R}_{nn}\left(\frac{x}{t}\right) = 0, \tag{3.16}$$

and also:

$$\tilde{R}_{n\tau}\left(\frac{x}{t}\right) = 0, \tag{3.17}$$

according to the realisability constraint (3.18):

$$R_{nn}R_{\tau\tau} - R_{n\tau}^2 \geq 0. \tag{3.18}$$

Therefore, system (2.2) becomes in this region:

$$\begin{cases} \partial_t \tilde{u}_n + \tilde{u}_n \partial_n \tilde{u}_n = 0, \\ \partial_t \tilde{u}_\tau + \tilde{u}_n \partial_n \tilde{u}_\tau = 0, \\ \partial_t \tilde{R}_{\tau\tau} + \tilde{u}_n \partial_n \tilde{R}_{\tau\tau} = 0, \end{cases} \tag{3.19}$$

with boundary condition  $\tilde{u}_n(\frac{x}{t} = u_n^-) = u_n^-$ ,  $\tilde{u}_\tau(\frac{x}{t} = u_n^-) = u_\tau^-$ ,  $\tilde{R}_{\tau\tau}(\frac{x}{t} = u_n^-) = R_{\tau\tau}^-$  (respectively:  $\tilde{u}_n(\frac{x}{t} = u_n^+) = u_n^+$ ,  $\tilde{u}_\tau(\frac{x}{t} = u_n^+) = u_\tau^+$ ,  $\tilde{R}_{\tau\tau}(\frac{x}{t} = u_n^+) = R_{\tau\tau}^+$ ).

Since  $u_n^- < u_n^+$  as seen in (3.11), the solution  $\tilde{u}_n(\frac{x}{t})$  of the first equation in (3.19) is given by:

$$\tilde{u}_n\left(\frac{x}{t}\right) = \frac{x}{t} \tag{3.20}$$

(that is the solution of Burgers equation in a rarefaction configuration).

The other components  $\tilde{u}_\tau(\frac{x}{t})$  and  $\tilde{R}_{\tau\tau}(\frac{x}{t})$  have yet to be defined in the non-turbulent region. Note first that any regular function  $\tilde{\phi}(\frac{x}{t})$  satisfies:

$$\partial_t \tilde{\phi} + \tilde{u}_n \partial_n \tilde{\phi} = \frac{1}{t} \left(\tilde{u}_n - \frac{x}{t}\right) \tilde{\phi}'\left(\frac{x}{t}\right) = 0, \tag{3.21}$$

inside the non-turbulent region, according to (3.20). Thus, there is no unique solution for  $\tilde{u}_\tau$  and  $\tilde{R}_{\tau\tau}$  in the non-turbulent region. It is similar to what is observed either in vacuum zones for the velocity field in the gas dynamics framework, or for the velocity field in dry zones for shallow-water equations.

A proposition to specify the variables  $\tilde{u}_\tau$  and  $\tilde{R}_{\tau\tau}$  in the non-turbulent region using a vanishing viscosity method (which is in fact present in the original system (1.1)), is discussed in Appendix C.

We can summarise the definition of the solution in the non-turbulent zones.

**Proposition 3.1** (Solution for the turbulent/non-turbulent connection).

The non-turbulent region is defined by  $\lambda_1(\mathbf{w}^-) < \frac{x}{t} < \lambda_5(\mathbf{w}^+)$ , where  $\lambda_1(\mathbf{w}^-) = u_n^-$  and  $\lambda_5(\mathbf{w}^+) = u_n^+$  are introduced through (3.7), (3.10), and where the edge states  $\mathbf{w}^-$  and  $\mathbf{w}^+$  are given by (3.14) and (3.15).

- The solution for  $\frac{x}{t} < \lambda_1(\mathbf{w}^L)$  (respectively for  $\frac{x}{t} > \lambda_5(\mathbf{w}^R)$ ) is given by relation (3.4) (respectively (3.5)). Inside the 1-rarefaction wave, for  $\lambda_1(\mathbf{w}^L) < \frac{x}{t} < \lambda_1(\mathbf{w}^-)$ , the solution is obtained through (3.8), whereas the solution inside the 5-rarefaction wave is given, for  $\lambda_5(\mathbf{w}^+) < \frac{x}{t} < \lambda_5(\mathbf{w}^R)$ , by (3.12).
- Inside the non-turbulent region for  $\lambda_1(\mathbf{w}^-) < \frac{x}{t} < \lambda_5(\mathbf{w}^+)$ , the solution for the variables  $\tilde{R}_{nn}$ ,  $\tilde{R}_{n\tau}$  and  $\tilde{u}_n$  is obtained with relations (3.16), (3.17), (3.20), whereas there is no unique solution for the variables  $\tilde{u}_\tau$  and  $\tilde{R}_{\tau\tau}$  in this region.

A special focus is also made in Appendix D in the case of non-turbulent initial data, which relies on the same ideas developed in this section.

#### 4. A GODUNOV-TYPE SCHEME USING GIVEN APPROXIMATE JUMP RELATIONS

The Riemann solver introduced in this section is a Godunov-type solver [22] based on the resolution of the exact Riemann problem associated with the convective subsystem (2.2). In the sequel we consider the relation (2.9) verified.

This resolution is applied to give the intermediate states at each cell interface. These values are then used to update the variables in the mesh scheme.

##### 4.1. Resolution of the Riemann problem at the interface

The resolution presented below is adapted from [21, 41].

###### 4.1.1. Exact form of intermediate states $u_n$ and $R_{nn}$

The Riemann invariants introduced in Section 2 enforce the following:

$$u_n^I = u_n^{II} = u_n^{III} = u_n^{IV} := u_n^*, \tag{4.1}$$

and:

$$R_{nn}^I = R_{nn}^{II} = R_{nn}^{III} = R_{nn}^{IV} := R_{nn}^*. \tag{4.2}$$

The approximate jump relations (2.7):

$$\begin{cases} \sigma[u_n]_l^r = \widehat{u}_n^{l|r} [u_n]_l^r + [R_{nn}]_l^r, \\ \sigma[R_{nn}]_l^r = 2\widehat{R}_{nn}^{l|r} [u_n]_l^r + \widehat{u}_n^{l|r} [R_{nn}]_l^r, \end{cases} \tag{4.3}$$

together with the Riemann invariants (2.6a) and (2.6e) associated with the two GNL waves:

$$\begin{cases} u_n^L + \sqrt{2R_{nn}^L} = u_n^* + \sqrt{2R_{nn}^*}, \\ u_n^* - \sqrt{2R_{nn}^*} = u_n^R - \sqrt{2R_{nn}^R}, \end{cases} \tag{4.4}$$

allow us to calculate  $u_n^*$  and  $R_{nn}^*$ .

The four configurations (e.g.,  $2^p$ , where  $p$  represents the number of GNL fields) must be taken into account, considering the left data  $\mathbf{w}^L$  and the right data  $\mathbf{w}^R$ .

Considering a wave separating the left ( $l$ ) and the right ( $r$ ) states, the ratio between the right and left normal components of the Reynolds tensor is denoted  $z = \frac{R_{nn}^r}{R_{nn}^l} > 0$ . Let us write the relations corresponding to the different admissible waves.

– For a 1-shock (respecting the entropy-like condition introduced in Appendix 2 of [24]), we have ( $z_1 > 1$ ):

$$\begin{cases} R_{nn}^* = z_1 R_{nn}^L, \\ u_n^* = u_n^L + \frac{1-z_1}{\sqrt{z_1+1}} \sqrt{R_{nn}^L}, \\ \sigma_1 = \frac{1}{2}(u_n^L + u_n^*) - \sqrt{R_{nn}^L + R_{nn}^*}. \end{cases} \tag{4.5}$$

– For a 1-rarefaction ( $0 < z_1 \leq 1$ ):

$$u_n^L = u_n^* - \sqrt{2R_{nn}^L}(1 - \sqrt{z_1 - 1}). \tag{4.6}$$

– For a 5-shock verifying the entropy condition ( $0 < z_5 < 1$ ), we have:

$$\begin{cases} R_{nn}^R = z_5 R_{nn}^*, \\ u_n^R = u_n^* + \frac{z_5-1}{\sqrt{z_5+1}} \sqrt{R_{nn}^*}, \\ \sigma_5 = \frac{1}{2}(u_n^* + u_n^R) + \sqrt{R_{nn}^* + R_{nn}^R}. \end{cases} \tag{4.7}$$

– For a 5-rarefaction ( $z_5 \geq 1$ ):

$$u_n^R = u_n^* + \sqrt{2R_{nn}^R} \left( 1 - \frac{1}{\sqrt{z_5}} \right). \tag{4.8}$$

These expressions can be gathered as follows:

$$\begin{cases} u_n^L = u_n^* - h_1(z_1) \sqrt{2R_{nn}^L}, & \text{with } z_1 = \frac{R_{nn}^*}{R_{nn}^L}, \\ u_n^R = u_n^* + h_5(z_5) \sqrt{2R_{nn}^R}, & \text{with } z_5 = \frac{R_{nn}^R}{R_{nn}^*}, \end{cases} \tag{4.9}$$

where  $h_1$  and  $h_5$  write:

$$h_1(z) = \begin{cases} \frac{1-z}{\sqrt{2(1+z)}}, & \text{if } z > 1, \\ 1 - \sqrt{z}, & \text{if } z \leq 1, \end{cases} \quad h_5(z) = \begin{cases} \frac{z-1}{\sqrt{2z(1+z)}}, & \text{if } z < 1, \\ 1 - \frac{1}{\sqrt{z}}, & \text{if } z \geq 1. \end{cases} \tag{4.10}$$

The left and right states can be therefore linked by the following relation:

$$u_n^R - u_n^L = h_5(z_5) \sqrt{2R_{nn}^R} + h_1(z_1) \sqrt{2R_{nn}^L}. \tag{4.11}$$

By noticing  $h_1(z) = h_5(1/z)$ , we have:

$$h_5(z_5) = h_5\left(\frac{R_{nn}^R}{R_{nn}^*}\right) = h_1\left(\frac{R_{nn}^*}{R_{nn}^R}\right) = h_1\left(\frac{R_{nn}^*}{R_{nn}^L} \frac{R_{nn}^L}{R_{nn}^R}\right) = h_1\left(z_1 \frac{R_{nn}^L}{R_{nn}^R}\right). \tag{4.12}$$

Thus, the connection relation (4.11) is equivalent to:

$$\Phi(z_1) := u_n^R - u_n^L - h_1\left(\frac{R_{nn}^L}{R_{nn}^R} z_1\right) \sqrt{2R_{nn}^R} - h_1(z_1) \sqrt{2R_{nn}^L} = 0. \tag{4.13}$$

The function  $h_1$  is regular for  $z > 0$  and strictly decreasing, so  $\Phi$  is strictly increasing. We also have:

$$\begin{cases} \Phi(0^+) = u_n^R - u_n^L - \sqrt{2R_{nn}^R} - \sqrt{2R_{nn}^L}, \\ \Phi(+\infty) = +\infty. \end{cases} \tag{4.14}$$

We note that  $\Phi(0^+) < 0$ , which corresponds to condition (2.9).

Thus, the solution  $z_1^*$  (and hence  $R_{nn}^*$  and  $u_n^*$  with (4.9)) exists and is unique according to the intermediate value theorem. If  $z_1^* \leq 1$ , the 1-wave is a 1-rarefaction, otherwise it is a 1-shock. If  $z_5^* = \frac{R_{nn}^R}{z_1^* R_{nn}^L} \geq 1$ , the 5-wave is a 5-rarefaction, otherwise it is a 5-shock.

4.1.2. Exact form of intermediate states  $u_\tau$ ,  $R_{n\tau}$  and  $R_{\tau\tau}$

The connection is established thanks to shock relations (2.7) and the Riemann invariants to determine all the variables in the half-plane  $(x, t > 0)$ .

– For a 1-shock wave ( $z_1^* > 1$ ), the state **I** writes as follows:

$$\begin{cases} u_\tau^I = u_\tau^L + \frac{1-z_1^*}{\sqrt{z_1^*+1}} \frac{R_{n\tau}^L}{\sqrt{R_{nn}^L}}, \\ R_{n\tau}^I = z_1^* R_{n\tau}^L, \\ R_{\tau\tau}^I = R_{\tau\tau}^L + (z_1^* - 1) \frac{(R_{n\tau}^L)^2}{R_{nn}^L}. \end{cases} \tag{4.15}$$

– For a 1-rarefaction wave ( $0 < z_1^* \leq 1$ ), the variables in the region **I** are determined using the Riemann invariants (2.6a):

$$\begin{cases} R_{n\tau}^I = R_{nn}^* \frac{R_{n\tau}^L}{R_{nn}^L}, \\ u_\tau^I = u_\tau^L + R_{n\tau}^L \sqrt{\frac{2}{R_{nn}^L}} - R_{n\tau}^I \sqrt{\frac{2}{R_{nn}^*}}, \\ R_{\tau\tau}^I = R_{\tau\tau}^L - \frac{(R_{n\tau}^L)^2}{R_{nn}^L} + \frac{(R_{n\tau}^I)^2}{R_{nn}^*}. \end{cases} \tag{4.16}$$

– For a 5-shock wave ( $0 < z_5^* < 1$ ) the state **IV** is determined as follows:

$$\begin{cases} R_{n\tau}^{IV} = \frac{R_{n\tau}^R}{z_5^*}, \\ u_\tau^{IV} = u_\tau^R - \frac{z_5^*-1}{\sqrt{z_5^*+1}} \frac{R_{n\tau}^{IV}}{\sqrt{R_{nn}^*}}, \\ R_{\tau\tau}^{IV} = R_{\tau\tau}^R - (z_5^* - 1) \frac{(R_{n\tau}^{IV})^2}{R_{nn}^*}. \end{cases} \tag{4.17}$$

– For 5-rarefaction wave ( $z_5^* \geq 1$ ), Riemann invariants (2.6e) give:

$$\begin{cases} R_{n\tau}^{IV} = R_{nn}^* \frac{R_{n\tau}^R}{R_{nn}^R}, \\ u_\tau^{IV} = u_\tau^R - R_{n\tau}^R \sqrt{\frac{2}{R_{nn}^R}} + R_{n\tau}^{IV} \sqrt{\frac{2}{R_{nn}^*}}, \\ R_{\tau\tau}^{IV} = R_{\tau\tau}^R - \frac{(R_{n\tau}^R)^2}{R_{nn}^R} + \frac{(R_{n\tau}^{IV})^2}{R_{nn}^*}. \end{cases} \tag{4.18}$$

Once the configuration and the variables for the states **I** and **IV** are determined, the invariants  $I_2^R$  (2.6b),  $I_3^R$  (2.6c) and  $I_4^R$  (2.6d) are used in the same way to determine the states **II** and **III**.

The Riemann invariants through the 3-wave  $I_3^R$  (2.6c) give:

$$\begin{cases} u_\tau^{II} = u_\tau^{III}, \\ R_{n\tau}^{II} = R_{n\tau}^{III}. \end{cases} \tag{4.19}$$

Using this relation and a linear combination of the equalities given by  $I_2^R$  (2.6b) and  $I_4^R$  (2.6d), we obtain the following.

$$\begin{cases} u_\tau^{\text{II}} = u_\tau^{\text{III}} = \frac{1}{2} \left( u_\tau^{\text{I}} + u_\tau^{\text{IV}} + \frac{R_{n\tau}^{\text{I}} - R_{n\tau}^{\text{IV}}}{\sqrt{R_{nn}^*}} \right), \\ R_{n\tau}^{\text{II}} = R_{n\tau}^{\text{III}} = \frac{R_{n\tau}^{\text{I}} + R_{n\tau}^{\text{IV}}}{2} + \sqrt{R_{nn}^*} \left( \frac{u_\tau^{\text{I}} - u_\tau^{\text{IV}}}{2} \right), \\ R_{\tau\tau}^{\text{II}} = R_{\tau\tau}^{\text{I}} - \frac{R_{n\tau}^{\text{I}^2} + R_{n\tau}^{\text{II}^2}}{R_{nn}^*}, \\ R_{\tau\tau}^{\text{III}} = R_{\tau\tau}^{\text{IV}} - \frac{R_{n\tau}^{\text{IV}^2} + R_{n\tau}^{\text{III}^2}}{R_{nn}^*}. \end{cases} \tag{4.20}$$

**Remark 4.1.**

- Assuming realisable left data  $w^L$  and right data  $w^R$ , all intermediate states  $R_{nn}$  are positive.
- Moreover, the Riemann invariant  $(R_{\tau\tau} - \frac{R_{n\tau}^2}{R_{nn}})$  in  $I_R^1$  and  $I_R^5$  guarantees positive values of  $(R_{nn}R_{\tau\tau} - R_{n\tau}^2)$  for states **I** and **IV**, if rarefaction waves occur.
- In addition, the approximate shock relations (4.15) give for state **I**:

$$\begin{aligned} R_{\tau\tau}^{\text{I}} &= R_{\tau\tau}^L + (z_1^* - 1) \frac{(R_{n\tau}^L)^2}{R_{nn}^L} = R_{\tau\tau}^L + \left( \frac{R_{n\tau}^{\text{I}}}{R_{n\tau}^L} - 1 \right) \frac{(R_{n\tau}^L)^2}{R_{nn}^L} \\ &= R_{\tau\tau}^L - \frac{(R_{n\tau}^L)^2}{R_{nn}^L} + R_{n\tau}^{\text{I}} \frac{R_{n\tau}^L}{R_{nn}^L} = R_{\tau\tau}^L - \frac{(R_{n\tau}^L)^2}{R_{nn}^L} + \frac{(R_{n\tau}^{\text{I}})^2}{R_{nn}^L}. \end{aligned} \tag{4.21}$$

This also provides a positive value of  $(R_{nn}^{\text{I}}R_{\tau\tau}^{\text{I}} - (R_{n\tau}^{\text{I}})^2)$  in the case of a 1-shock since  $R_{nn}^{\text{I}} > 0$ . A similar result is obtained in the case of a 5-shock for state **IV** using relations (4.17) and  $R_{nn}^{\text{IV}} > 0$ .

- Eventually, the Riemann invariant  $(R_{nn}R_{\tau\tau} - R_{n\tau}^2)$  in  $I_R^2$  and  $I_R^4$  guarantees the realisability of the intermediate Reynolds stress tensor through the 2- and 4-LD waves, for states **II** and **III**.

**4.2. Mesh scheme**

In the sequel, we propose a mesh scheme to compute the approximate solution of system (2.2). We will verify in Section 6 the convergence towards the correct solutions.

We consider a one-dimensional mesh whose cells are segments  $s_i, i \in \mathcal{I}$ . Each segment  $s_i$  is centred at  $x_i$  and has 2 interfaces  $x_{i+1/2}$  and  $x_{i-1/2}$  shared with the segments  $s_{i+1}$  and  $s_{i-1}$ . We denote  $\phi_i^N$  the value of a quantity  $\phi$  averaged in the segment  $s_i$  and taken at time  $t^N$ . We introduce the explicit resolution at each time step  $t^N$  in three phases:

- **Step 1 (Loop on interfaces):** A one-dimensional Riemann problem is solved at each interface  $x_{i+1/2}$  where the appropriate values of the variables of interest  $w_{i+1/2}^N$  are determined at the interface considering left data  $w_i^N$  and right data  $w_{i+1}^N$ . The calculation of the intermediate states is processed as seen in the previous paragraph and the state at the interface is affected to  $w_{i+1/2}^N$ .
- **Step 2 (Time step  $\delta t^N$  calculation):** The time step  $\delta t^N = t^{N+1} - t^N$  is calculated in accordance with a CFL condition considering the fastest wave speed arising from the Riemann problems at cell interfaces:

$$\delta t^N = \text{CFL} \frac{1}{\max_{i,k} \left( \frac{|\lambda_{k,i-1/2}^N|}{\delta x_i}, \frac{|\lambda_{k,i+1/2}^N|}{\delta x_i} \right)}, \tag{4.22}$$

where  $\lambda_{k,i+1/2}^N$ ,  $k = 1, \dots, 5$ , correspond to the speed waves (2.5) arising from the Riemann problem resolution between states  $\mathbf{w}_i^N$  and  $\mathbf{w}_{i+1}^N$  at time  $t^N$ . The value of CFL will be fixed, close to, and smaller than 1/2. A similar remark holds for the relaxation scheme introduced in Section 5.

- **Step 3 (Loop on cells):** Starting with  $\mathbf{w}_i^N$  inside cell  $x_i$  and noting  $\delta x_i = x_{i+1/2} - x_{i-1/2}$ , the variable is updated at time  $t^{N+1}$  to  $\mathbf{w}_i^{N+1}$  taking interface contributions  $\mathbf{w}_{i+1/2}^N$  and  $\mathbf{w}_{i-1/2}^N$  into account.

We consider the following explicit mesh scheme:

$$\begin{cases} \delta x_i (u_{ni}^{N+1} - u_{ni}^N) + \delta t^N (\widehat{u}_{ni}^N \Delta_i(u_n^N) + \Delta_i(R_{nn}^N)) = 0, \\ \delta x_i (R_{nni}^{N+1} - R_{nni}^N) + \delta t^N (\widehat{u}_{ni}^N \Delta_i(R_{nn}^N) + 2\widehat{R}_{nni}^N \Delta_i(u_n^N)) = 0, \\ \delta x_i (u_{\tau i}^{N+1} - u_{\tau i}^N) + \delta t^N (\widehat{u}_{ni}^N \Delta_i(u_\tau^N) + \Delta_i(R_{n\tau}^N)) = 0, \\ \delta x_i (R_{n\tau i}^{N+1} - R_{n\tau i}^N) + \delta t^N (\widehat{u}_{ni}^N \Delta_i(R_{n\tau}^N) + \widehat{R}_{nni}^N \Delta_i(u_\tau^N) + \widehat{R}_{n\tau i}^N \Delta_i(u_n^N)) = 0, \\ \delta x_i (R_{\tau\tau i}^{N+1} - R_{\tau\tau i}^N) + \delta t^N (\widehat{u}_{ni}^N \Delta_i(R_{\tau\tau}^N) + 2\widehat{R}_{n\tau i}^N \Delta_i(u_\tau^N)) = 0, \end{cases} \quad (4.23)$$

where, for any scalar  $\phi$ :

$$\begin{cases} \widehat{\phi}_i = \frac{\phi_{i+1/2} + \phi_{i-1/2}}{2}, \\ \Delta_i(\phi) = \phi_{i+1/2} - \phi_{i-1/2}. \end{cases} \quad (4.24)$$

$\phi_{i+1/2}^N$  stands for any component of  $\mathbf{w}_{i+1/2}^N$  that is the solution at the interface  $x_{i+1/2}$  of the Riemann problem between the left state  $\mathbf{w}_i^N$  and the right state  $\mathbf{w}_{i+1}^N$  at time  $t^N$ :

$$\phi_{i+1/2}^N = \phi \left( \mathbf{w}^{\text{Riemann}} \left( \frac{x - x_{i+1/2}}{t} = 0, \mathbf{w}^L = \mathbf{w}_i^N, \mathbf{w}^R = \mathbf{w}_{i+1}^N \right) \right). \quad (4.25)$$

The treatment of non-conservative products in this mesh scheme is identical to that of Forestier *et al.* [18], Berthon *et al.* [2] in the context of turbulent compressible flows or Dolejší and Gallouët [14] for two-phase flows. When considering non-conservative models with non-conservative products active in GNL fields (two-phase flow models, shallow water models, turbulent flow models), other numerical integration methods have been proposed to handle non-conservative products (see Appendix F, [6–8, 29, 33, 35, 39]).

## 5. A RELAXATION SCHEME FOR THE TWO-DIMENSIONAL RESOLUTION

This section explores an explicit method whose aim is to maintain high accuracy as for the Godunov-type explicit scheme and to reduce computational cost. The approach follows the main ideas introduced in [5, 9, 10, 12, 25, 30, 42], and is based on an evolution system that is augmented with a transport equation of a relaxation variable  $\mathcal{R}$ . This evolution system is expected to describe a dynamics similar to that of system (2.2), but without any GNL field. The evolution step is supplemented with an instantaneous relaxation step, where the relaxation variable  $\mathcal{R}$  is enforced to  $R_{nn}$  at the end of each time step.

### 5.1. The augmented evolution system

The following evolution system, is adapted from the convective subsystem (2.2). It reads:

$$\begin{cases} \partial_t u_n + u_n \partial_n u_n + \partial_n \Pi(R_{nn}, \mathcal{R}) = 0, \\ \partial_t R_{nn} + u_n \partial_n R_{nn} + 2R_{nn} \partial_n u_n = 0, \\ \partial_t \mathcal{R} + u_n \partial_n \mathcal{R} = 0, \\ \partial_t u_\tau + u_n \partial_n u_\tau + \partial_n R_{n\tau} = 0, \\ \partial_t R_{n\tau} + u_n \partial_n R_{n\tau} + R_{nn} \partial_n u_\tau + R_{n\tau} \partial_n u_n = 0, \\ \partial_t R_{\tau\tau} + u_n \partial_n R_{\tau\tau} + 2R_{n\tau} \partial_n u_\tau = 0. \end{cases} \quad (5.1)$$

We denote  $\mathbf{W} = (u_n, R_{nn}, \mathcal{R}, u_\tau, R_{n\tau}, R_{\tau\tau})^T$ . The relaxation Reynolds tensor normal component is denoted by  $\mathcal{R}$ . We consider the so-called relaxed Reynolds tensor normal component:

$$\Pi(R_{nn}, \mathcal{R}) = \mathcal{R} + a^2(\mathcal{R}^{-1} - R_{nn}^{-1}), \tag{5.2}$$

with  $\Pi(R_{nn}, R_{nn}) = R_{nn}$ . The positive parameter  $a$  has the same dimension as a Reynolds tensor component. The conditions that the parameter  $a$  must satisfy are introduced further, considering the Whitham condition (see [5, 9, 10, 12, 25, 30, 42]).

The relaxation variable  $\mathcal{R}$  of the Reynolds stress tensor normal component is introduced through a transport equation.

### 5.2. Analysis of the augmented evolution system

The unknown vector  $\mathbf{W}$  satisfies:

$$\partial_t \mathbf{W} + \mathbf{C}(\mathbf{W}) \partial_n \mathbf{W} = \mathbf{0}, \tag{5.3}$$

with

$$\mathbf{C}(\mathbf{W}) = \begin{pmatrix} u_n & \frac{\partial \Pi}{\partial R_{nn}} & \frac{\partial \Pi}{\partial \mathcal{R}} & 0 & 0 & 0 \\ 2R_{nn} & u_n & 0 & 0 & 0 & 0 \\ 0 & 0 & u_n & 0 & 0 & 0 \\ 0 & 0 & 0 & u_n & 1 & 0 \\ R_{n\tau} & 0 & 0 & R_{nn} & u_n & 0 \\ 0 & 0 & 0 & 2R_{n\tau} & 0 & u_n \end{pmatrix}. \tag{5.4}$$

We have:

**Proposition 5.1** (Hyperbolicity of system (5.1)).

– The eigenvalues of  $\mathbf{C}$  read:

$$\begin{cases} \lambda_1^{\text{RS}} = u_n - a\sqrt{2}R_{nn}^{-1/2}, & \lambda_2^{\text{RS}} = u_n - \sqrt{R_{nn}}, \\ \lambda_{3,4}^{\text{RS}} = u_n, \\ \lambda_5^{\text{RS}} = u_n + \sqrt{R_{nn}}, & \lambda_6^{\text{RS}} = u_n + a\sqrt{2}R_{nn}^{-1/2}. \end{cases} \tag{5.5}$$

– The associated right eigenvectors are given by:

$$\left\{ \begin{aligned} \mathbf{r}_1 &= \left( 1, -\frac{\sqrt{2}R_{nn}^{3/2}}{a}, 0, \frac{R_{n\tau}R_{nn}}{2a^2 - R_{nn}^2}, -\frac{\sqrt{2}aR_{n\tau}R_{nn}^{1/2}}{2a^2 - R_{nn}^2}, -\frac{\sqrt{2}R_{n\tau}^2R_{nn}^{3/2}}{a(2a^2 - R_{nn}^2)} \right)^T, \\ \mathbf{r}_2 &= (0, 0, 0, 1, -R_{nn}^{1/2}, -2R_{nn}^{-1/2}R_{n\tau})^T, \\ \mathbf{r}_3 &= (0, -\frac{\partial \Pi}{\partial \mathcal{R}}, \frac{\partial \Pi}{\partial R_{nn}}, 0, 0, 0)^T, \\ \mathbf{r}_4 &= (0, -\frac{\partial \Pi}{\partial \mathcal{R}}, \frac{\partial \Pi}{\partial R_{nn}}, 0, 0, 1)^T, \\ \mathbf{r}_5 &= (0, 0, 0, 1, R_{nn}^{1/2}, 2R_{nn}^{-1/2}R_{n\tau})^T, \\ \mathbf{r}_6 &= \left( 1, +\frac{\sqrt{2}R_{nn}^{3/2}}{a}, 0, \frac{R_{n\tau}R_{nn}}{2a^2 - R_{nn}^2}, \frac{\sqrt{2}aR_{n\tau}R_{nn}^{1/2}}{2a^2 - R_{nn}^2}, \frac{\sqrt{2}R_{n\tau}^2R_{nn}^{3/2}}{a(2a^2 - R_{nn}^2)} \right)^T, \end{aligned} \right. \tag{5.6}$$

and span  $\mathbb{R}^6$ .

Having satisfied this condition and  $R_{nn}$  being positive, the augmented evolution system (5.1) is hyperbolic.

*Proof.* The proof is straightforward. □

In order to satisfy a stability condition for relaxation schemes, the waves of the augmented evolution system are expected to encompass those of the classical system according to the Whitham condition (see [5, 9, 10, 12, 25, 30, 42]). Thus, the parameter  $a$  must satisfy:

$$a > R_{nn}. \tag{5.7}$$

This condition will be examined more precisely in Proposition 5.4 of Section 5.2.2.

We now focus on the structure of each field for system (5.1).

**Proposition 5.2** (Structure of fields in (5.1)). *All fields of system (5.1) are linearly degenerate.*

*Proof.* – Considering  $\mathbf{W} = (u_n, R_{nn}, \mathcal{R}, u_\tau, R_{n\tau}, R_{\tau\tau})^T$ , one immediately obtains:

$$\nabla_{\mathbf{W}}(\lambda_k^{\text{RS}}) \cdot \mathbf{r}_k = 0, \quad \text{for } k = 2, 3, 4, 5. \tag{5.8}$$

– For  $k = 1$ , we have:

$$\begin{aligned} \nabla_{\mathbf{W}}(\lambda_1^{\text{RS}})^T \cdot \mathbf{r}_1 &= (1, \frac{aR_{nn}^{-3/2}}{\sqrt{2}}, 0, 0, 0, 0) \cdot \mathbf{r}_1 = 1 - \frac{aR_{nn}^{-3/2}}{\sqrt{2}} \times \left( \frac{\sqrt{2}R_{nn}^{3/2}}{a} \right) \\ &= 0. \end{aligned} \tag{5.9}$$

– For  $k = 6$ , we similarly have:

$$\nabla_{\mathbf{W}}(\lambda_6^{\text{RS}}) \cdot \mathbf{r}_6 = 0. \tag{5.10}$$

□

### 5.2.1. Riemann invariants within each field

In the following, we list the Riemann invariants within each field.

**Proposition 5.3** (Riemann invariants in system (5.1)). *We denote by  $J_R^k$  the list of Riemann invariants through the  $k$ -wave for system (5.1). Then we have:*

$$J_R^1 = \left\{ u_n - a\sqrt{\frac{2}{R_{nn}}}, R_{\tau\tau} - \frac{R_{n\tau}^2}{R_{nn}}, \frac{R_{n\tau}}{\sqrt{R_{nn}}}(2a^2 - R_{nn}^2)^{1/4}, u_\tau + \sqrt{2}\frac{R_{n\tau}}{\sqrt{R_{nn}}}\eta\left(\frac{R_{nn}}{a}\right), \mathcal{R} \right\}, \tag{5.11a}$$

$$J_R^2 = \left\{ u_n, R_{nn}, R_{nn}R_{\tau\tau} - R_{n\tau}^2, u_\tau + \frac{R_{n\tau}}{\sqrt{R_{nn}}}, \mathcal{R} \right\}, \tag{5.11b}$$

$$J_R^{3,4} = \left\{ u_n, \Pi(R_{nn}, \mathcal{R}), u_\tau, R_{n\tau} \right\}, \tag{5.11c}$$

$$J_R^5 = \left\{ u_n, R_{nn}, R_{nn}R_{\tau\tau} - R_{n\tau}^2, u_\tau - \frac{R_{n\tau}}{\sqrt{R_{nn}}}, \mathcal{R} \right\}, \tag{5.11d}$$

$$J_R^6 = \left\{ u_n + a\sqrt{\frac{2}{R_{nn}}}, R_{\tau\tau} - \frac{R_{n\tau}^2}{R_{nn}}, \frac{R_{n\tau}}{\sqrt{R_{nn}}}(2a^2 - R_{nn}^2)^{1/4}, u_\tau - \sqrt{2}\frac{R_{n\tau}}{\sqrt{R_{nn}}}\eta\left(\frac{R_{nn}}{a}\right), \mathcal{R} \right\}, \tag{5.11e}$$

where the dimensionless function  $\eta$  satisfies the following ODE:

$$\text{For } x \in [0, \sqrt{2}]: \begin{cases} \eta'(x) + \frac{x}{2(2-x^2)}\eta(x) = \frac{1}{2(2-x^2)}, \\ \eta(1) = 1. \end{cases} \tag{5.12}$$

*Proof.* One can verify that for every  $j_R^k \in J_R^k$ , we have  $\nabla_{\mathbf{W}}(j_R^k) \cdot \mathbf{r}_k = 0, k = 1, \dots, 6.$  □

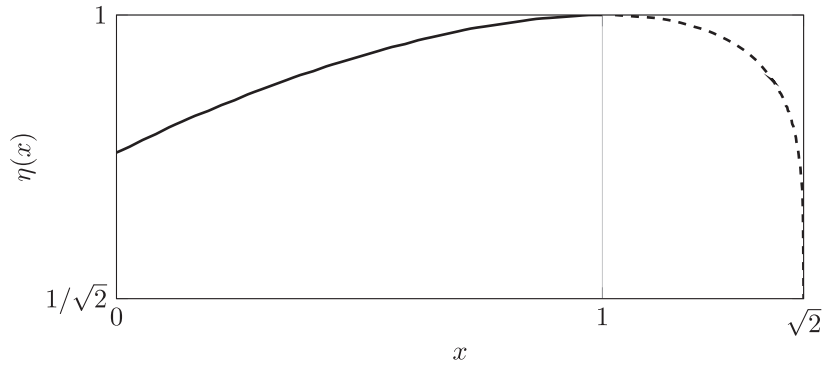


FIGURE 4. Plot of function  $\eta$  for  $x$  in  $[0, \sqrt{2})$ .

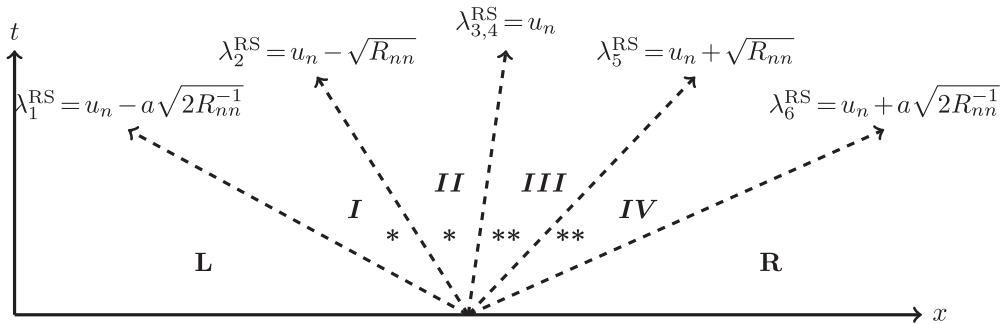


FIGURE 5. Augmented evolution system (5.1) intermediate states, all waves are LD (represented by dashed arrows).

We plot in Figure 4 the values of the function  $\eta$  in  $[0, \sqrt{2})$ .

**Remark 5.1.**

- The argument  $\frac{R_{nn}}{a}$  always belongs to the domain of definition of  $\eta$  when the Whitham condition is satisfied.
- The quantity  $\frac{R_{n\tau}}{\sqrt{R_{nn}}}$  which appears in several Riemann invariants is bounded. Indeed, for realisable data, we have:

$$\frac{|R_{n\tau}|}{\sqrt{R_{nn}}} < \sqrt{R_{\tau\tau}}. \tag{5.13}$$

- One can also notice that  $J_R^2 = I_R^2 \cup \{\mathcal{R}\}$  and  $J_R^5 = I_R^4 \cup \{\mathcal{R}\}$ .

5.2.2. Exact form of  $u_n$ ,  $R_{nn}$  and  $\mathcal{R}$  intermediate states

The intermediate states arising from the resolution of the Riemann problem associated with (5.1) are depicted in Figure 5.

The Riemann invariants give  $u_n$  uniform in the regions **I**, **II**, **III** and **IV**. Variables  $\mathcal{R}$  and  $R_{nn}$  are uniform in **I**, **II** angular sectors and uniform in **III**, **IV** angular sectors, hence we denote:

$$\begin{cases} u_n^I = u_n^{II} = u_n^{III} = u_n^{IV} := u_n^*, \\ R_{nn}^I = R_{nn}^{II} := R_{nn}^*, \\ R_{nn}^{III} = R_{nn}^{IV} := R_{nn}^{**}, \end{cases} \tag{5.14}$$

and also:

$$\begin{cases} \mathcal{R}^I = \mathcal{R}^{II} := \mathcal{R}^*, \\ \mathcal{R}^{III} = \mathcal{R}^{IV} := \mathcal{R}^{**}. \end{cases} \tag{5.15}$$

After calculation using Riemann invariants in  $J_R^1$  (5.11a),  $J_R^{3,4}$  (5.11c) and  $J_R^6$  (5.11e), one obtains:

$$\begin{cases} u_n^* = \frac{[\frac{1}{2}u_n^2 - \Pi(R_{nn}, \mathcal{R})]_L^R + 2\sqrt{2}a \left( \widehat{u_n R_{nn}^{-1/2}}^{L|R} \right)}{[u_n]_L^R + 2\sqrt{2}a \left( \widehat{R_{nn}^{-1/2}}^{L|R} \right)}, \\ R_{nn}^{*-1} = \left( R_{nn}^{L-1/2} + \frac{1}{\sqrt{2}a} (u_n^* - u_n^L) \right)^2, \\ R_{nn}^{** -1} = \left( R_{nn}^{R-1/2} + \frac{1}{\sqrt{2}a} (u_n^R - u_n^*) \right)^2, \end{cases} \tag{5.16}$$

together with (5.15):

$$\begin{cases} \mathcal{R}^* = \mathcal{R}^L, \\ \mathcal{R}^{**} = \mathcal{R}^R, \end{cases} \tag{5.17}$$

where we recall  $[\phi]_L^R := \phi^R - \phi^L$  and  $\widehat{\phi}^{L|R} := \frac{1}{2}(\phi^L + \phi^R)$  for any quantity  $\phi$ .

**Remark 5.2.**

- One can notice that  $R_{nn}^*$  and  $R_{nn}^{**}$  are positive whatever the realisable left and right states  $\mathbf{W}_L$  and  $\mathbf{W}_R$  are.
- Assume that  $a$  is sufficiently large, then:

$$\begin{cases} u_n^* \sim \frac{\left( \widehat{u_n R_{nn}^{-1/2}}^{L|R} \right)}{\left( \widehat{R_{nn}^{-1/2}}^{L|R} \right)}, \\ R_{nn}^{*-1} \sim R_{nn}^{L-1}, \\ R_{nn}^{** -1} \sim R_{nn}^{R-1}. \end{cases} \tag{5.18}$$

- Moreover, for  $a > 0$ , we check that  $\mathbf{W}_L = \mathbf{W}_R$  implies  $u_n^* = u_n^L = u_n^R$  and  $R_{nn}^* = R_{nn}^{**} = R_{nn}^L = R_{nn}^R$ .

Thus, for  $a$  large enough, and for any realisable left and right states  $\mathbf{W}_L$  and  $\mathbf{W}_R$ , intermediate states are well defined and:

$$\lambda_6^{RS}(\mathbf{W}^R) - \lambda_1^{RS}(\mathbf{W}^L) = u_n^R - u_n^L + a \left( \sqrt{\frac{2}{R_{nn}^R}} + \sqrt{\frac{2}{R_{nn}^L}} \right) > 0, \tag{5.19}$$

which corresponds to the denominator appearing in the calculation of  $u_n^*$  in (5.16).

TABLE 1. Case 1 initial data.

	$u_n$	$R_{nn}$	$u_\tau$	$R_{n\tau}$	$R_{\tau\tau}$
$L$	0	0.5	1	-0.1	0.5
$R$	0	0.5	1	0.1	0.5

**Proposition 5.4** (Wave ordering in the augmented evolution system (5.1)). *Let  $\mathbf{W}_L$  and  $\mathbf{W}_R$  be two realisable constant states such that the existence and uniqueness of the solution of the initial problem (2.2) are guaranteed. Assume that  $a > 0$  satisfies the conditions:*

$$\begin{cases} u_n^R - u_n^L + a \left( \sqrt{\frac{2}{R_{nn}^R}} + \sqrt{\frac{2}{R_{nn}^L}} \right) = \lambda_6^{\text{RS}}(\mathbf{W}^R) - \lambda_1^{\text{RS}}(\mathbf{W}^L) > 0, \\ a > \max(R_{nn}^L, R_{nn}^R, R_{nn}^*, R_{nn}^{**}). \end{cases} \tag{5.20}$$

Then, the waves arising from the augmented evolution system (5.1) are well-ordered, such that:

$$\lambda_1^{\text{RS}}(\mathbf{W}^L) < \lambda_2^{\text{RS}}(\mathbf{W}^*) < \lambda_{3,4}^{\text{RS}}(\mathbf{W}^*) < \lambda_5^{\text{RS}}(\mathbf{W}^{**}) < \lambda_6^{\text{RS}}(\mathbf{W}^R). \tag{5.21}$$

*Proof.* The Riemann invariants in  $J_R^6$  (5.11e) give:

$$\lambda_6^{\text{RS}}(\mathbf{W}^R) = u_n^* + a \sqrt{\frac{2}{R_{nn}^{**}}} > u_n^* + \sqrt{R_{nn}^{**}} = \lambda_5^{\text{RS}}(\mathbf{W}^{**}), \tag{5.22}$$

as soon as:

$$a > \frac{R_{nn}^{**}}{\sqrt{2}}, \tag{5.23}$$

which holds true, owing to (5.20). In the same way, using the Riemann invariants in  $J_R^1$  (5.11a), we have:

$$\lambda_1^{\text{RS}}(\mathbf{W}^L) = u_n^* - a \sqrt{\frac{2}{R_{nn}^*}} < u_n^* - \sqrt{R_{nn}^*} = \lambda_2^{\text{RS}}(\mathbf{W}^*), \tag{5.24}$$

as soon as:

$$a > \frac{R_{nn}^*}{\sqrt{2}}. \tag{5.25}$$

Eventually, since  $\lambda_{3,4}^{\text{RS}}(\mathbf{W}^*) = u_n^*$ , the ordering is complete. □

### 5.2.3. Exact form of $u_\tau$ , $R_{n\tau}$ and $R_{\tau\tau}$ intermediate states

The Riemann invariants in  $J_R^1$  and  $J_R^6$  are used to obtain  $R_{n\tau}$ , then  $u_\tau$  and  $R_{\tau\tau}$  in regions **I** and **IV**:

$$\begin{cases} R_{n\tau}^I = R_{n\tau}^L \left( \frac{2a^2 - R_{nn}^{L2}}{R_{nn}^{L2}} \right)^{1/4} \left( \frac{2a^2 - R_{nn}^{*2}}{R_{nn}^{*2}} \right)^{-1/4}, \\ u_\tau^I = u_\tau^L + R_{n\tau}^L \sqrt{\frac{2}{R_{nn}^L}} \eta \left( \frac{R_{nn}^L}{a} \right) - R_{n\tau}^I \sqrt{\frac{2}{R_{nn}^*}} \eta \left( \frac{R_{nn}^*}{a} \right), \\ R_{\tau\tau}^I = R_{\tau\tau}^L - \frac{R_{n\tau}^{L2}}{R_{nn}^L} + \frac{R_{n\tau}^{I2}}{R_{nn}^*}, \end{cases} \tag{5.26}$$

TABLE 2. Case 1 relative  $L^1$  errors and convergence rates  $\alpha$ .

	$N_c$	$u_n$		$R_{nn}$		$u_\tau$		$R_{n\tau}$		$R_{\tau\tau}$	
		Err	$\alpha$	Err	$\alpha$	Err	$\alpha$	Err	$\alpha$	Err	$\alpha$
Godunov-type	100	0		0		$6.52 \times 10^{-3}$		$5.60 \times 10^{-2}$		$3.20 \times 10^{-3}$	
	200	0		0		$4.50 \times 10^{-3}$	0.54	$3.91 \times 10^{-2}$	0.52	$2.15 \times 10^{-3}$	0.57
	400	0		0		$3.16 \times 10^{-3}$	0.51	$2.74 \times 10^{-2}$	0.51	$1.52 \times 10^{-3}$	0.51
	800	0		0		$2.22 \times 10^{-3}$	0.51	$1.94 \times 10^{-2}$	0.50	$1.04 \times 10^{-3}$	0.54
	1600	0		0		$1.57 \times 10^{-3}$	0.50	$1.37 \times 10^{-2}$	0.50	$7.56 \times 10^{-4}$	0.46
	3200	0		0		$1.11 \times 10^{-3}$	0.50	$9.66 \times 10^{-3}$	0.50	$5.29 \times 10^{-4}$	0.52
	6400	0		0		$7.84 \times 10^{-4}$	0.50	$6.83 \times 10^{-3}$	0.50	$3.68 \times 10^{-4}$	0.52
RS	100	0		0		$6.52 \times 10^{-3}$		$5.60 \times 10^{-2}$		$3.20 \times 10^{-3}$	
	200	0		0		$4.50 \times 10^{-3}$	0.54	$3.91 \times 10^{-2}$	0.52	$2.15 \times 10^{-3}$	0.57
	400	0		0		$3.16 \times 10^{-3}$	0.51	$2.74 \times 10^{-2}$	0.51	$1.52 \times 10^{-3}$	0.51
	800	0		0		$2.22 \times 10^{-3}$	0.51	$1.94 \times 10^{-2}$	0.50	$1.04 \times 10^{-3}$	0.54
	1600	0		0		$1.57 \times 10^{-3}$	0.50	$1.37 \times 10^{-2}$	0.50	$7.56 \times 10^{-4}$	0.46
	3200	0		0		$1.11 \times 10^{-3}$	0.50	$9.66 \times 10^{-3}$	0.50	$5.29 \times 10^{-4}$	0.52
	6400	0		0		$7.84 \times 10^{-4}$	0.50	$6.83 \times 10^{-3}$	0.50	$3.68 \times 10^{-4}$	0.52
Rusanov	100	0		0		$8.17 \times 10^{-3}$		$7.01 \times 10^{-2}$		$4.46 \times 10^{-3}$	
	200	0		0		$5.68 \times 10^{-3}$	0.52	$4.93 \times 10^{-2}$	0.51	$2.97 \times 10^{-3}$	0.59
	400	0		0		$3.99 \times 10^{-3}$	0.51	$3.47 \times 10^{-2}$	0.51	$2.04 \times 10^{-3}$	0.54
	800	0		0		$2.81 \times 10^{-3}$	0.50	$2.45 \times 10^{-2}$	0.50	$1.39 \times 10^{-3}$	0.56
	1600	0		0		$1.99 \times 10^{-3}$	0.50	$1.73 \times 10^{-2}$	0.50	$9.86 \times 10^{-4}$	0.49
	3200	0		0		$1.41 \times 10^{-3}$	0.50	$1.22 \times 10^{-2}$	0.50	$6.85 \times 10^{-4}$	0.53
	6400	0		0		$9.93 \times 10^{-4}$	0.50	$8.65 \times 10^{-3}$	0.50	$4.75 \times 10^{-4}$	0.53

and:

$$\begin{cases} R_{n\tau}^{IV} = R_{n\tau}^R \left( \frac{2a^2 - R_{nn}^R}{R_{nn}^R} \right)^{1/4} \left( \frac{2a^2 - R_{nn}^{**}}{R_{nn}^{**}} \right)^{-1/4}, \\ u_\tau^{IV} = u_\tau^R - R_{n\tau}^R \sqrt{\frac{2}{R_{nn}^R}} \eta \left( \frac{R_{nn}^R}{a} \right) + R_{n\tau}^{IV} \sqrt{\frac{2}{R_{nn}^{**}}} \eta \left( \frac{R_{nn}^{**}}{a} \right), \\ R_{\tau\tau}^{IV} = R_{\tau\tau}^R - \frac{R_{n\tau}^R{}^2}{R_{nn}^R} + \frac{R_{n\tau}^{IV}{}^2}{R_{nn}^{**}}. \end{cases} \tag{5.27}$$

The invariants in  $J_R^{3,4}$  give  $u_\tau^{II} = u_\tau^{III}$  and  $R_{n\tau}^{II} = R_{n\tau}^{III}$ . Using  $J_R^2$  (5.11b) and  $J_R^5$  (5.11d),  $u_\tau$  and  $R_{n\tau}$  are fully determined:

$$\begin{cases} R_{n\tau}^{II} = R_{n\tau}^{III} = \left( R_{n\tau}^I \sqrt{\frac{1}{R_{nn}^*}} + R_{n\tau}^{IV} \sqrt{\frac{1}{R_{nn}^{**}}} + u_\tau^I - u_\tau^{IV} \right) \left( \sqrt{\frac{1}{R_{nn}^*}} + \sqrt{\frac{1}{R_{nn}^{**}}} \right)^{-1}, \\ u_\tau^{II} = u_\tau^{III} = \frac{1}{2} (u_\tau^I + u_\tau^{IV}) + \frac{1}{2} \left( \frac{R_{n\tau}^I}{\sqrt{R_{nn}^*}} - \frac{R_{n\tau}^{IV}}{\sqrt{R_{nn}^{**}}} \right) + \frac{1}{2} R_{n\tau}^{II} \left( \sqrt{\frac{1}{R_{nn}^{**}}} - \sqrt{\frac{1}{R_{nn}^*}} \right). \end{cases} \tag{5.28}$$

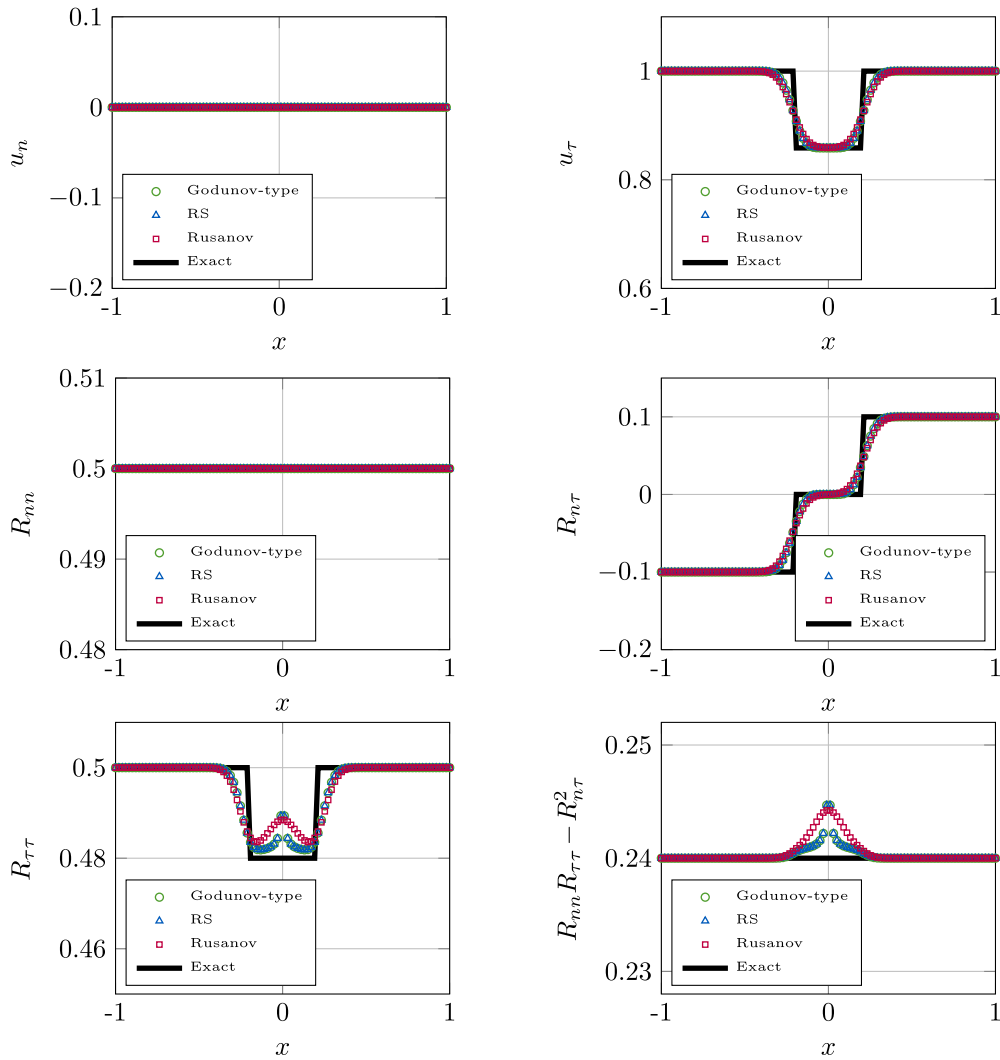


FIGURE 6. Case 1 numerical solutions with  $N_c = 100$ ,  $t_f = 0.3 \frac{\mathcal{L}}{\sqrt{2R_{nn}^L}}$ .

TABLE 3. Case 2 initial data.

	$u_n$	$R_{nn}$	$u_\tau$	$R_{n\tau}$	$R_{\tau\tau}$
$L$	1	0.5	1	0.1	0.5
$R$	1	0.5	1	0.1	0.8

Eventually, the intermediate component  $R_{\tau\tau}$  is obtained in regions **II** and **III** using the invariants in  $J_R^2$  and  $J_R^5$ :

$$\begin{cases} R_{\tau\tau}^{\text{II}} = R_{\tau\tau}^{\text{I}} - \frac{R_{n\tau}^{\text{I}2} - R_{n\tau}^{\text{II}2}}{R_{nn}^*}, \\ R_{\tau\tau}^{\text{III}} = R_{\tau\tau}^{\text{IV}} - \frac{R_{n\tau}^{\text{IV}2} - R_{n\tau}^{\text{III}2}}{R_{nn}^{**}}. \end{cases} \tag{5.29}$$

TABLE 4. Case 2 relative  $L^1$  errors and convergence rates  $\alpha$ .

	$N_c$	$u_n$		$R_{nn}$		$u_\tau$		$R_{n\tau}$		$R_{\tau\tau}$	
		Err	$\alpha$	Err	$\alpha$	Err	$\alpha$	Err	$\alpha$	Err	$\alpha$
Godunov-type	100	0		0		0		0		$1.35 \times 10^{-2}$	
	200	0		0		0		0		$9.55 \times 10^{-3}$	0.50
	400	0		0		0		0		$6.75 \times 10^{-3}$	0.50
	800	0		0		0		0		$4.77 \times 10^{-3}$	0.50
	1600	0		0		0		0		$3.38 \times 10^{-3}$	0.50
	3200	0		0		0		0		$2.39 \times 10^{-3}$	0.50
	6400	0		0		0		0		$1.69 \times 10^{-3}$	0.50
RS	100	0		0		0		0		$1.35 \times 10^{-2}$	
	200	0		0		0		0		$9.55 \times 10^{-3}$	0.50
	400	0		0		0		0		$6.75 \times 10^{-3}$	0.50
	800	0		0		0		0		$4.77 \times 10^{-3}$	0.50
	1600	0		0		0		0		$3.38 \times 10^{-3}$	0.50
	3200	0		0		0		0		$2.39 \times 10^{-3}$	0.50
	6400	0		0		0		0		$1.69 \times 10^{-3}$	0.50
Rusanov	100	0		0		0		0		$2.04 \times 10^{-2}$	
	200	0		0		0		0		$1.44 \times 10^{-2}$	0.50
	400	0		0		0		0		$1.02 \times 10^{-2}$	0.50
	800	0		0		0		0		$7.22 \times 10^{-3}$	0.50
	1600	0		0		0		0		$5.11 \times 10^{-3}$	0.50
	3200	0		0		0		0		$3.61 \times 10^{-3}$	0.50
	6400	0		0		0		0		$2.55 \times 10^{-3}$	0.50

TABLE 5. Case 3 initial data.

	$u_n$	$R_{nn}$	$u_\tau$	$R_{n\tau}$	$R_{\tau\tau}$
$L$	1	7	1	0.6	2
$R$	3	3	2	1.3	8

**Proposition 5.5** (Realisability of intermediate states). *The augmented evolution system (5.1) provides realisable intermediate states.*

*Proof.* – According to (5.16),  $R_{nn}$  is positive in the intermediate regions considering realisable left and right data.

– Moreover, for realisable left and right data, just as in the resolution of the exact problem (2.2), the positiveness of  $R_{nn}R_{\tau\tau} - R_{n\tau}^2$  is propagated throughout the half-plane  $(x, t > 0)$  due to the Riemann invariants  $R_{\tau\tau} - \frac{R_{n\tau}^2}{R_{nn}}$  in  $J_R^1$  and  $J_R^6$  and  $R_{nn}R_{\tau\tau} - R_{n\tau}^2$  in  $J_R^2$  and  $J_R^5$ .

Hence, the realisability of the intermediate Reynolds tensors is guaranteed. □

The main results describing the solution of the Riemann problem associated with (5.1) can be gathered in:

**Proposition 5.6** (Solution of the Riemann problem associated with the augmented evolution system (5.1)). *Assume realisable left and right states  $\mathbf{W}_L$  and  $\mathbf{W}_R$ , and that  $a > 0$  is such that (5.20) holds, then the realisable*

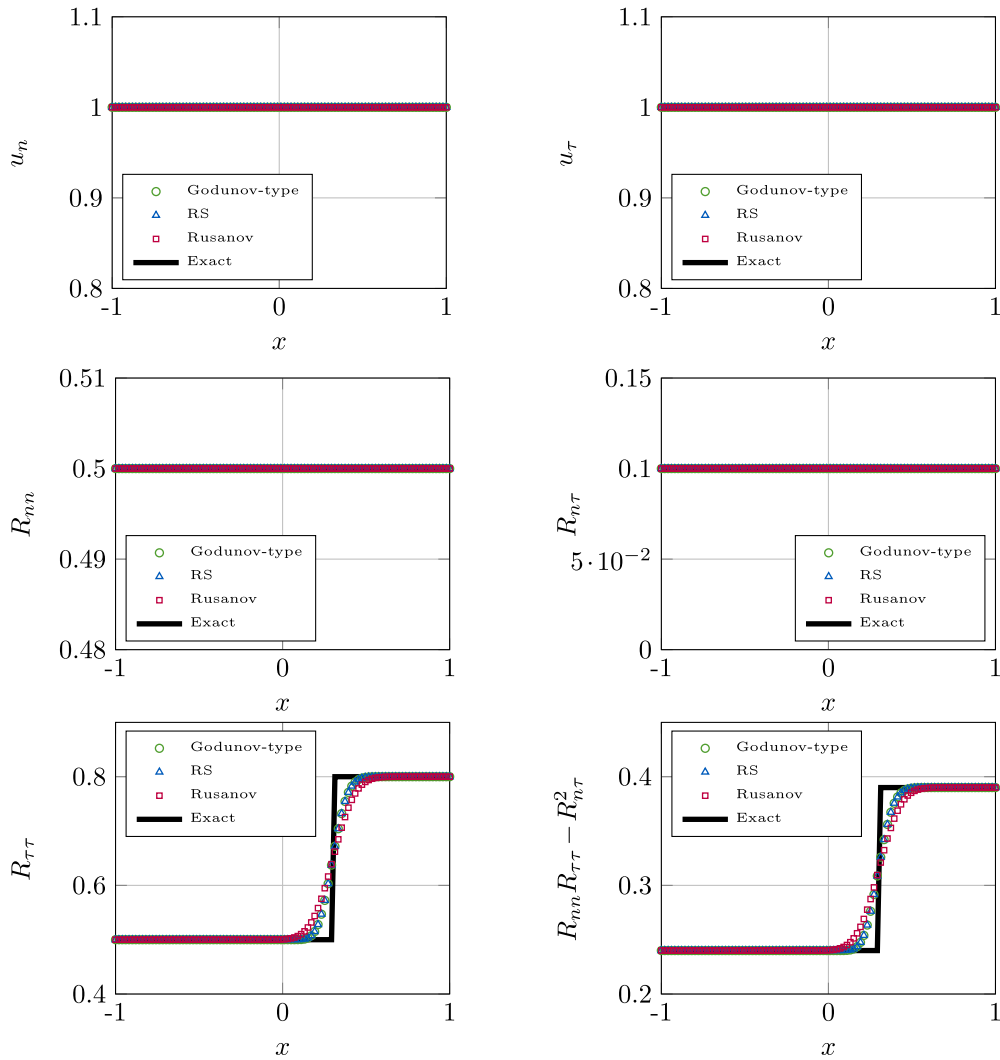


FIGURE 7. Case 2 numerical solutions with  $N_c = 100$ ,  $t_f = 0.3 \frac{\mathcal{L}}{\sqrt{2R_n^L}}$ .

self-similar solution  $\mathbf{W}(x, t) = \widetilde{\mathbf{W}}\left(\frac{x}{t}\right)$  of the augmented evolution system (5.1) reads:

$$\widetilde{\mathbf{W}}\left(\frac{x}{t}\right) = \begin{cases} \mathbf{W}^L & \text{if } \frac{x}{t} < \lambda_1^{\text{RS}}(\mathbf{W}^L), \\ \mathbf{W}^I & \text{if } \lambda_1^{\text{RS}}(\mathbf{W}^L) < \frac{x}{t} < \lambda_2^{\text{RS}}(\mathbf{W}^*), \\ \mathbf{W}^{II} & \text{if } \lambda_2^{\text{RS}}(\mathbf{W}^*) < \frac{x}{t} < \lambda_{3,4}^{\text{RS}}(\mathbf{W}^*), \\ \mathbf{W}^{III} & \text{if } \lambda_{3,4}^{\text{RS}}(\mathbf{W}^*) < \frac{x}{t} < \lambda_5^{\text{RS}}(\mathbf{W}^{**}), \\ \mathbf{W}^{IV} & \text{if } \lambda_5^{\text{RS}}(\mathbf{W}^{**}) < \frac{x}{t} < \lambda_6^{\text{RS}}(\mathbf{W}^R), \\ \mathbf{W}^R & \text{if } \frac{x}{t} > \lambda_6^{\text{RS}}(\mathbf{W}^R), \end{cases} \tag{5.30}$$

TABLE 6. Case 3 relative  $L^1$  errors and convergence rates  $\alpha$ .

	$N_c$	$u_n$		$R_{nn}$		$u_\tau$		$R_{n\tau}$		$R_{\tau\tau}$	
		Err	$\alpha$	Err	$\alpha$	Err	$\alpha$	Err	$\alpha$	Err	$\alpha$
Godunov-type	100	$1.43 \times 10^{-2}$		$1.82 \times 10^{-2}$		$1.96 \times 10^{-2}$		$6.49 \times 10^{-2}$		$3.82 \times 10^{-2}$	
	200	$9.28 \times 10^{-3}$	0.63	$1.17 \times 10^{-2}$	0.64	$1.37 \times 10^{-2}$	0.52	$4.47 \times 10^{-2}$	0.54	$2.70 \times 10^{-2}$	0.50
	400	$5.93 \times 10^{-3}$	0.65	$7.41 \times 10^{-3}$	0.66	$9.65 \times 10^{-3}$	0.51	$3.11 \times 10^{-2}$	0.52	$1.92 \times 10^{-2}$	0.49
	800	$3.72 \times 10^{-3}$	0.67	$4.61 \times 10^{-3}$	0.68	$6.64 \times 10^{-3}$	0.54	$2.18 \times 10^{-2}$	0.51	$1.35 \times 10^{-2}$	0.51
	1600	$2.29 \times 10^{-3}$	0.70	$2.82 \times 10^{-3}$	0.71	$4.79 \times 10^{-3}$	0.47	$1.58 \times 10^{-2}$	0.46	$9.63 \times 10^{-3}$	0.49
	3200	$1.38 \times 10^{-3}$	0.73	$1.69 \times 10^{-3}$	0.74	$3.33 \times 10^{-3}$	0.53	$1.09 \times 10^{-2}$	0.53	$6.84 \times 10^{-3}$	0.49
	6400	$8.20 \times 10^{-4}$	0.75	$9.96 \times 10^{-4}$	0.76	$2.24 \times 10^{-3}$	0.57	$7.33 \times 10^{-3}$	0.58	$4.83 \times 10^{-3}$	0.50
	12800	$4.78 \times 10^{-4}$	0.78	$5.78 \times 10^{-4}$	0.79	$1.52 \times 10^{-3}$	0.56	$4.92 \times 10^{-3}$	0.57	$3.41 \times 10^{-3}$	0.50
RS	100	$1.60 \times 10^{-2}$		$2.02 \times 10^{-2}$		$2.02 \times 10^{-2}$		$6.73 \times 10^{-2}$		$3.85 \times 10^{-2}$	
	200	$9.93 \times 10^{-3}$	0.69	$1.25 \times 10^{-2}$	0.69	$1.42 \times 10^{-2}$	0.51	$4.66 \times 10^{-2}$	0.53	$2.71 \times 10^{-2}$	0.51
	400	$6.13 \times 10^{-3}$	0.69	$7.67 \times 10^{-3}$	0.70	$9.94 \times 10^{-3}$	0.51	$3.20 \times 10^{-2}$	0.54	$1.93 \times 10^{-2}$	0.49
	800	$3.75 \times 10^{-3}$	0.71	$4.67 \times 10^{-3}$	0.72	$6.80 \times 10^{-3}$	0.55	$2.22 \times 10^{-2}$	0.53	$1.36 \times 10^{-2}$	0.51
	1600	$2.26 \times 10^{-3}$	0.73	$2.80 \times 10^{-3}$	0.74	$4.87 \times 10^{-3}$	0.48	$1.60 \times 10^{-2}$	0.48	$9.64 \times 10^{-3}$	0.49
	3200	$1.35 \times 10^{-3}$	0.74	$1.66 \times 10^{-3}$	0.75	$3.36 \times 10^{-3}$	0.54	$1.10 \times 10^{-2}$	0.53	$6.85 \times 10^{-3}$	0.49
	6400	$7.98 \times 10^{-4}$	0.76	$9.74 \times 10^{-4}$	0.77	$2.25 \times 10^{-3}$	0.58	$7.35 \times 10^{-3}$	0.58	$4.83 \times 10^{-3}$	0.50
	12800	$4.64 \times 10^{-4}$	0.78	$5.63 \times 10^{-4}$	0.79	$1.52 \times 10^{-3}$	0.57	$4.92 \times 10^{-3}$	0.58	$3.41 \times 10^{-3}$	0.50
Rusanov	100	$2.87 \times 10^{-2}$		$3.70 \times 10^{-2}$		$2.58 \times 10^{-2}$		$8.72 \times 10^{-2}$		$6.11 \times 10^{-2}$	
	200	$1.86 \times 10^{-2}$	0.62	$2.36 \times 10^{-2}$	0.65	$1.81 \times 10^{-2}$	0.51	$6.09 \times 10^{-2}$	0.52	$4.11 \times 10^{-2}$	0.57
	400	$1.18 \times 10^{-2}$	0.66	$1.47 \times 10^{-2}$	0.68	$1.27 \times 10^{-2}$	0.51	$4.23 \times 10^{-2}$	0.53	$2.84 \times 10^{-2}$	0.53
	800	$7.27 \times 10^{-3}$	0.70	$9.00 \times 10^{-3}$	0.71	$8.68 \times 10^{-3}$	0.55	$2.88 \times 10^{-2}$	0.55	$1.95 \times 10^{-2}$	0.54
	1600	$4.39 \times 10^{-3}$	0.73	$5.39 \times 10^{-3}$	0.74	$6.18 \times 10^{-3}$	0.49	$2.07 \times 10^{-2}$	0.48	$1.36 \times 10^{-2}$	0.53
	3200	$2.60 \times 10^{-3}$	0.76	$3.17 \times 10^{-3}$	0.77	$4.32 \times 10^{-3}$	0.52	$1.43 \times 10^{-2}$	0.53	$9.56 \times 10^{-3}$	0.50
	6400	$1.51 \times 10^{-3}$	0.78	$1.83 \times 10^{-3}$	0.79	$2.90 \times 10^{-3}$	0.57	$9.59 \times 10^{-3}$	0.58	$6.72 \times 10^{-3}$	0.51
	12800	$8.65 \times 10^{-4}$	0.81	$1.04 \times 10^{-3}$	0.81	$1.96 \times 10^{-3}$	0.57	$6.40 \times 10^{-3}$	0.58	$4.74 \times 10^{-3}$	0.51

TABLE 7. Case 4 initial data.

	$u_n$	$R_{nn}$	$u_\tau$	$R_{n\tau}$	$R_{\tau\tau}$
$L$	$-0.99 \times \sqrt{2}$	1	1	-0.1	0.5
$R$	$0.99 \times \sqrt{2}$	1	1	0.1	0.5

with  $\lambda_{3,4}^{RS}(\mathbf{W}^*) = \lambda_{3,4}^{RS}(\mathbf{W}^{**}) = u_n^*$ .

- The intermediate states  $u_n$ ,  $R_{nn}$ , and  $\mathcal{R}$  are given in the regions **I**, **II**, **III** and **IV** using relations (5.14), (5.15), (5.16) and (5.17).
- The intermediate states  $u_\tau$ ,  $R_{n\tau}$ ,  $R_{\tau\tau}$  are given in the region **I** using (5.26), in region **IV** using (5.27) and in regions **II** and **III** using (5.28) and (5.29).

*Proof.* The calculations are left to the reader, who can use the Riemann invariants as explained above. □

### 5.3. Mesh scheme

The numerical implementation of the mesh scheme is carried out as in Section 4.2. A tabulation of the  $\eta$  function according to (5.12) is provided once and for all at the start of the code.

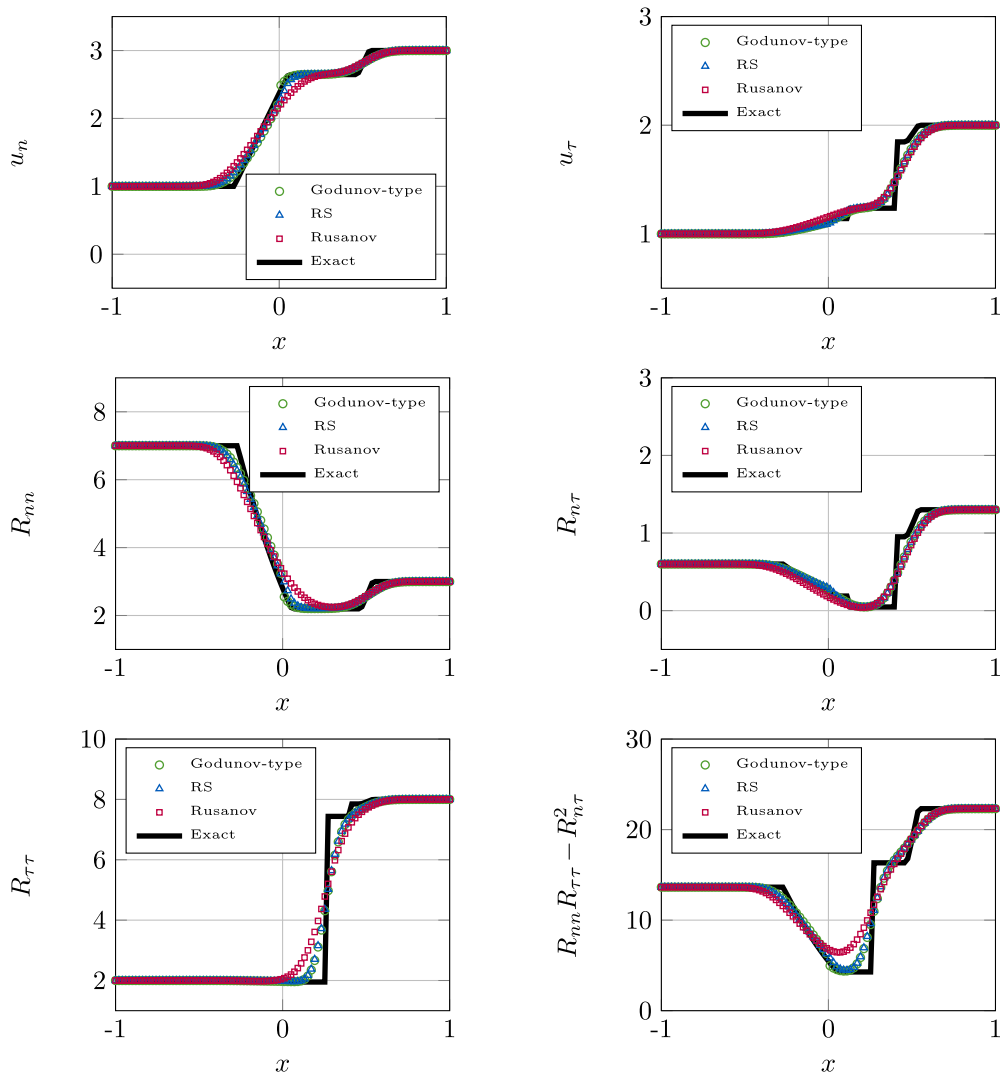


FIGURE 8. Case 3 numerical solutions with  $N_c = 100$ ,  $t_f = 0.1$  s.

At each time step  $t^N$ , the resolution involves a Riemann problem resolution of the augmented evolution system (5.1) at each interface  $x_{i+1/2}$  with an initial control of parameter  $a$  according to (5.20):

$$a_{i+1/2}^N = (1 + \epsilon_a) \max \left( R_{nni}^N, R_{nni+1}^N, \frac{u_{ni}^N - u_{ni+1}^N}{\left( \sqrt{\frac{2}{R_{nni+1}^N}} + \sqrt{\frac{2}{R_{nni}^N}} \right)} \right). \tag{5.31}$$

**Remark 5.3.** In a first stance, the left and right states can be such that the intermediate values  $R_{nn}^*$  or  $R_{nn}^{**}$  emerging from the resolution are greater than the parameter  $a_{i+1/2}^N$ . However it is always possible to increase

TABLE 8. Case 4 relative  $L^1$  errors and convergence rates  $\alpha$ .

	$N_c$	$u_n$		$R_{nn}$		$u_\tau$		$R_{n\tau}$		$R_{\tau\tau}$	
		Err	$\alpha$	Err	$\alpha$	Err	$\alpha$	Err	$\alpha$	Err	$\alpha$
Godunov-type	100	$3.80 \times 10^{-2}$		$6.02 \times 10^{-2}$		$3.45 \times 10^{-3}$		$5.24 \times 10^{-2}$		$6.90 \times 10^{-4}$	
	200	$2.38 \times 10^{-2}$	0.68	$3.63 \times 10^{-2}$	0.73	$2.30 \times 10^{-3}$	0.58	$3.02 \times 10^{-2}$	0.79	$4.06 \times 10^{-4}$	0.77
	400	$1.44 \times 10^{-2}$	0.72	$2.14 \times 10^{-2}$	0.76	$1.58 \times 10^{-3}$	0.54	$1.79 \times 10^{-2}$	0.75	$2.57 \times 10^{-4}$	0.66
	800	$8.56 \times 10^{-3}$	0.75	$1.25 \times 10^{-2}$	0.77	$1.12 \times 10^{-3}$	0.50	$1.09 \times 10^{-2}$	0.72	$1.75 \times 10^{-4}$	0.56
	1600	$4.99 \times 10^{-3}$	0.78	$7.21 \times 10^{-3}$	0.80	$8.12 \times 10^{-4}$	0.46	$6.77 \times 10^{-3}$	0.69	$1.21 \times 10^{-4}$	0.53
	3200	$2.86 \times 10^{-3}$	0.80	$4.09 \times 10^{-3}$	0.82	$6.25 \times 10^{-4}$	0.38	$4.28 \times 10^{-3}$	0.66	$8.42 \times 10^{-5}$	0.53
	6400	$1.63 \times 10^{-3}$	0.82	$2.29 \times 10^{-3}$	0.83	$4.96 \times 10^{-4}$	0.34	$2.73 \times 10^{-3}$	0.64	$5.81 \times 10^{-5}$	0.54
	12800	$9.17 \times 10^{-4}$	0.83	$1.27 \times 10^{-3}$	0.85	$3.96 \times 10^{-4}$	0.32	$1.76 \times 10^{-3}$	0.63	$3.96 \times 10^{-5}$	0.55
RS	100	$3.58 \times 10^{-2}$		$6.27 \times 10^{-2}$		$4.52 \times 10^{-3}$		$6.65 \times 10^{-2}$		$1.29 \times 10^{-3}$	
	200	$2.29 \times 10^{-2}$	0.64	$3.71 \times 10^{-2}$	0.75	$3.02 \times 10^{-3}$	0.58	$4.26 \times 10^{-2}$	0.64	$9.00 \times 10^{-4}$	0.52
	400	$1.41 \times 10^{-2}$	0.70	$2.17 \times 10^{-2}$	0.77	$2.18 \times 10^{-3}$	0.47	$2.69 \times 10^{-2}$	0.66	$6.17 \times 10^{-4}$	0.54
	800	$8.47 \times 10^{-3}$	0.74	$1.26 \times 10^{-2}$	0.78	$1.60 \times 10^{-3}$	0.45	$1.69 \times 10^{-2}$	0.67	$4.18 \times 10^{-4}$	0.56
	1600	$4.96 \times 10^{-3}$	0.77	$7.22 \times 10^{-3}$	0.81	$1.18 \times 10^{-3}$	0.44	$1.05 \times 10^{-2}$	0.68	$2.80 \times 10^{-4}$	0.58
	3200	$2.86 \times 10^{-3}$	0.80	$4.08 \times 10^{-3}$	0.82	$8.73 \times 10^{-4}$	0.43	$6.57 \times 10^{-3}$	0.68	$1.86 \times 10^{-4}$	0.59
	6400	$1.63 \times 10^{-3}$	0.81	$2.29 \times 10^{-3}$	0.84	$6.51 \times 10^{-4}$	0.42	$4.12 \times 10^{-3}$	0.67	$1.23 \times 10^{-4}$	0.60
	12800	$9.16 \times 10^{-4}$	0.83	$1.27 \times 10^{-3}$	0.85	$4.89 \times 10^{-4}$	0.41	$2.60 \times 10^{-3}$	0.66	$8.22 \times 10^{-5}$	0.58
Rusanov	100	$3.61 \times 10^{-2}$		$6.70 \times 10^{-2}$		$1.10 \times 10^{-2}$		$8.51 \times 10^{-2}$		$4.36 \times 10^{-3}$	
	200	$2.25 \times 10^{-2}$	0.68	$3.89 \times 10^{-2}$	0.78	$7.71 \times 10^{-3}$	0.51	$6.01 \times 10^{-2}$	0.50	$3.31 \times 10^{-3}$	0.40
	400	$1.37 \times 10^{-2}$	0.72	$2.24 \times 10^{-2}$	0.80	$5.33 \times 10^{-3}$	0.53	$4.12 \times 10^{-2}$	0.54	$2.44 \times 10^{-3}$	0.44
	800	$8.13 \times 10^{-3}$	0.75	$1.29 \times 10^{-2}$	0.80	$3.66 \times 10^{-3}$	0.54	$2.79 \times 10^{-2}$	0.56	$1.76 \times 10^{-3}$	0.47
	1600	$4.75 \times 10^{-3}$	0.78	$7.29 \times 10^{-3}$	0.82	$2.48 \times 10^{-3}$	0.56	$1.86 \times 10^{-2}$	0.59	$1.25 \times 10^{-3}$	0.50
	3200	$2.73 \times 10^{-3}$	0.80	$4.10 \times 10^{-3}$	0.83	$1.83 \times 10^{-3}$	0.44	$1.23 \times 10^{-2}$	0.60	$8.73 \times 10^{-4}$	0.50
	6400	$1.55 \times 10^{-3}$	0.81	$2.28 \times 10^{-3}$	0.84	$1.43 \times 10^{-3}$	0.35	$8.14 \times 10^{-3}$	0.60	$6.02 \times 10^{-4}$	0.53
	12800	$8.76 \times 10^{-4}$	0.83	$1.26 \times 10^{-3}$	0.86	$1.13 \times 10^{-3}$	0.34	$5.41 \times 10^{-3}$	0.59	$4.11 \times 10^{-4}$	0.55

parameter  $a_{i+1/2}^N$  so that:

$$\begin{cases} u_{ni+1}^N - u_{ni}^N + a_{i+1/2}^N \left( \sqrt{\frac{2}{R_{nni+1}^N}} + \sqrt{\frac{2}{R_{nni}^N}} \right) = \lambda_6^{\text{RS}}(\mathbf{W}_{i+1}^N) - \lambda_1^{\text{RS}}(\mathbf{W}_i^N) > 0, \\ a_{i+1/2}^N > \max(R_{nni}^N, R_{nni+1}^N, R_{nn}^*, R_{nn}^{**}), \end{cases} \tag{5.32}$$

in compliance with the wave ordering condition and the Whitham condition (5.20).

In practice, we take  $\epsilon_a = 10^{-2}$  in Section 6.

Then a calculation of the time step  $\delta t^N$  according to a CFL condition similar to (4.22) is carried out before eventually the updating of the variables using the contribution at the interfaces.

We recall that, in practice, an instantaneous relaxation step is considered, which consists in initialising for all cells the relaxation variable  $(\mathcal{R})_i^N$  at each time step  $t^N$  at the value of  $(R_{nn})_i^N$ .

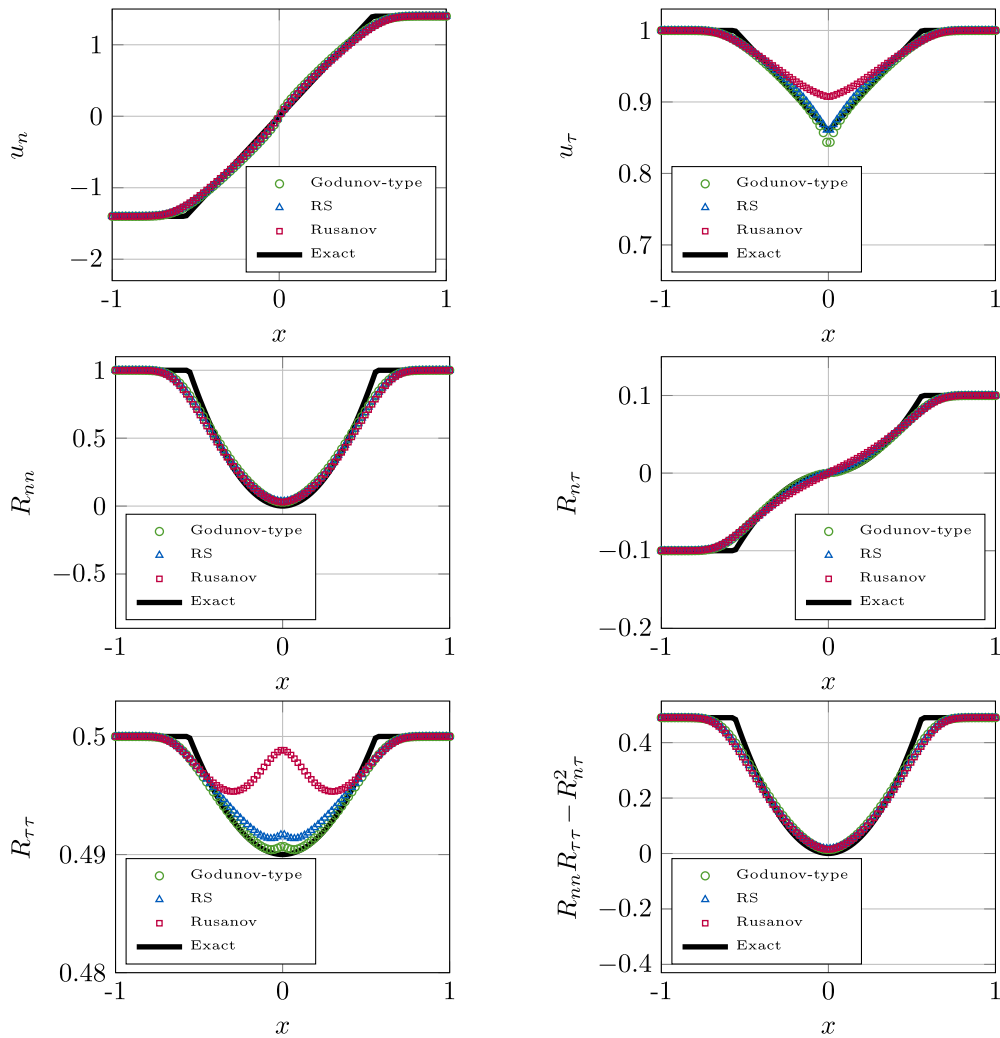


FIGURE 9. Case 4 numerical solutions with  $N_c = 100$ ,  $t_f = 0.2 \frac{\mathcal{L}}{\sqrt{R_{nn}^L}}$ .

The following relaxation mesh scheme, denoted RS in the sequel, is implemented (using the same notations as in (4.24)):

$$\begin{cases}
 \delta x_i (u_{ni}^{N+1} - u_{ni}^N) + \delta t^N \left( \widehat{u}_{ni}^N \Delta_i(u_n^N) + \Pi(R_{nni+1/2}^N, \mathcal{R}_{i+1/2}^N) - \Pi(R_{nni-1/2}^N, \mathcal{R}_{i-1/2}^N) \right) = 0, \\
 \delta x_i (R_{nni}^{N+1} - R_{nni}^N) + \delta t^N \left( \widehat{u}_{ni}^N \Delta_i(R_{nn}^N) + 2\widehat{R}_{nni}^N \Delta_i(u_n^N) \right) = 0, \\
 \delta x_i (u_{\tau i}^{N+1} - u_{\tau i}^N) + \delta t^N \left( \widehat{u}_{ni}^N \Delta_i(u_\tau^N) + \Delta_i(R_{n\tau}^N) \right) = 0, \\
 \delta x_i (R_{n\tau i}^{N+1} - R_{n\tau i}^N) + \delta t^N \left( \widehat{u}_{ni}^N \Delta_i(R_{n\tau}^N) + \widehat{R}_{nni}^N \Delta_i(u_\tau^N) + \widehat{R}_{n\tau i}^N \Delta_i(u_n^N) \right) = 0, \\
 \delta x_i (R_{\tau\tau i}^{N+1} - R_{\tau\tau i}^N) + \delta t^N \left( \widehat{u}_{ni}^N \Delta_i(R_{\tau\tau}^N) + 2\widehat{R}_{n\tau i}^N \Delta_i(u_\tau^N) \right) = 0,
 \end{cases} \tag{5.33}$$

This updating precedes the instantaneous relaxation step:

$$\mathcal{R}_i^{N+1} = R_{nni}^{N+1}. \tag{5.34}$$

## 6. VERIFICATION TEST CASES

We focus now on four distinct Riemann problems.

For all simulations, we consider regular meshes with a constant mesh size  $\delta x = 2\mathcal{L}/N_c$ , where  $N_c$  is the number of cells, and the characteristic size of the domain  $\mathcal{L}$  is 1 metre. We also take CFL = 0.45 in the sequel.

At  $t = 0$ , we consider the initial conditions of a Riemann problem with  $\mathbf{w}(x < 0, t = 0) = \mathbf{w}^L$  and  $\mathbf{w}(x > 0, t = 0) = \mathbf{w}^R$  that will be recalled for each test case. All velocities are expressed in metres per second, and Reynolds stresses are expressed in metres per second squared.

The Godunov-type scheme and the relaxation scheme (RS) will be compared with a Rusanov scheme (see [38]) in tables in which we give the  $L^1$  relative error and associated convergence rates  $\alpha$ . We also plot the numerical solution associated to the three schemes for  $N_c = 100$  at a time  $t_f$ .

A test case showing an apparition of a non-turbulent region is discussed in Appendix C.2.

### 6.1. Test case 1: near-wall flow with three LD waves

This test case is taken from [17]. The initial conditions in this test case, recalled in Table 1, are representative of what happens in the vicinity of a wall boundary. They are such that  $u_n^L = -u_n^R \leq 0$ ,  $R_{nn}^L = R_{nn}^R$ ,  $u_\tau^L = u_\tau^R$ ,  $R_{n\tau}^L = -R_{n\tau}^R$ , and  $R_{\tau\tau}^L = R_{\tau\tau}^R$ . In this specific case, due to the initial values  $u_n^L = u_n^R = 0$ , the 1-wave and 5-wave in system (2.2) are ghost waves, *i.e.*, waves through which none of our variables varies. This particularity is retrieved by the three schemes, even on coarse meshes (see Fig. 6). The behaviour through the two LD waves corresponding to the 2-wave and 4-wave is monotonous, and these waves enforce convergence rates  $\alpha \simeq 1/2$  (see Tab. 2), as expected (see [19]). Eventually, we note a small standard glitch around the initial interface located at  $x = 0$  (corresponding to the LD 3-wave).

The Godunov-type and relaxation schemes lead to a similar error on a given mesh size. We note in Table 2 almost the same error between the Rusanov-type and the Godunov-type/RS schemes for twice finer meshes.

### 6.2. Test case 2: Riemann problem with a single contact discontinuity

The initial conditions recalled in Table 3 are such that the 1-wave, the 2-wave, the 4-wave and the 5-wave arising in the exact self-similar solution of system (2.2) are ghost waves. The behaviour of  $R_{\tau\tau}$  through the 3-wave travelling at speed  $\frac{x}{t} = 1$  is still monotonous as seen in Figure 7. The error arising through the 3-wave with the Rusanov scheme is still higher considering a given mesh size, as confirmed in Table 4, and is approximately the same as the Godunov-type/RS scheme errors for twice finer meshes.

### 6.3. Test case 3: general Riemann problem

In this test case, the initial conditions, recalled in Table 5, comply with realisability and (2.9). We plot the numerical solutions associated to the three schemes in Figure 8.

Focusing on variables  $u_n$  and  $R_{nn}$ , in Table 6 we observe that the three schemes converge at a slightly lower rate than 1. Actually, these variables converge well to the exact solution at an order close to the theoretical order  $\alpha = 1$ , which is expected for the three schemes because  $u_n$  and  $R_{nn}$  are preserved through the 2–3–4 LD waves according to (2.6b), (2.6c), and (2.6d). The observed order of 0.8 is in line with convergence speeds on a mesh of the same size for an Euler-type system (see [19]). The Godunov-type scheme gives approximately the same error as RS and is twice more accurate than the Rusanov scheme for a given mesh size.

The last three variables  $u_\tau$ ,  $R_{n\tau}$ ,  $R_{\tau\tau}$ , which also vary through the 2–3–4 LD waves, have a similar convergence rate close to  $\alpha = 1/2$ .

#### 6.4. Test case 4: near-wall flow with almost non-turbulent region

As in the first test case, the initial conditions in this test, recalled in Table 7, case are representative of what happens close to a wall boundary.

The initial values are such that  $u_n^R - u_n^L = 0.99(\sqrt{2R_{nn}^R} + \sqrt{2R_{nn}^L})$ , so that condition (2.9) is nearly violated. The resulting intermediate state  $R_{nn}^*$  is small as seen in Figure 9, more precisely:  $R_{nn}^* \simeq 5 \times 10^{-4}$ . The solution is obviously symmetrical (respectively, antisymmetrical) for variables with symmetrical (respectively, antisymmetrical) initial conditions.

We retrieve similar convergence rates in Table 8, close to 1, for variables  $u_n$  and  $R_{nn}$ . In addition, all three schemes give similar errors for these variables.

The convergence rates observed on the finer meshes for the variables  $R_{n\tau}$  and  $R_{\tau\tau}$  are again of the order of  $\alpha = 1/2$ .

For the variable  $u_\tau$ , the convergence rates observed on the finer meshes are a bit smaller than the one expected  $\alpha = 1/2$ .

### 7. CONCLUDING REMARKS

Numerical schemes dealing with the convective part of a class of second-order turbulence-moment model of the Reynolds averaged Navier–Stokes equations for incompressible flows are presented in this paper. They have been developed in order to allow a better stabilisation in the numerical treatment of this system of equations. We have presented a Godunov-type scheme and a relaxation scheme, in Sections 4 and 5 respectively. Both perform similarly in terms of accuracy and provide expected convergence rates in turbulent zones when comparing to Riemann problem solutions. This provides numerical tools allowing to compute the approximate solution  $(\bar{\mathbf{u}}^\#, \mathbf{R}^\#)$  in the first step (1.3) more accurately than with a Rusanov scheme [17], when considering “ideal” turbulence as introduced in [46] and in [47], Chapter 5.

When non-turbulent regions occur, the unique solution for the normal velocity  $u_n$ , the normal Reynolds stress  $R_{nn}$ , and the Reynolds shear  $R_{n\tau}$  components has been defined in these areas and compared with the approximate solutions (see Appendices C, D, E). Further investigation is necessary in order to better understand the behaviour of the tangential velocity  $u_\tau$  and the tangential Reynolds stress  $R_{\tau\tau}$  components in the emerging non-turbulent regions.

The algorithm presented in this paper for the resolution of second-order turbulence-moment transport equations and the methods developed for processing the convective subsystem are currently being implemented in the code `saturne` CFD code. We recall that similar methodologies have been used for turbulent compressible flow models (see [6]), and more recently in the shear shallow water framework (see [4, 20, 31, 44]).

Furthermore, the wall (respectively inlet/outlet) boundary conditions can be accounted for by applying the classical mirror state (respectively half Riemann problem, see [16]) technique, and the solution of the one-dimensional Riemann problem recalled in this paper.

For future work, other closure models, as well as the analysis of the discrete-level realisability of the Reynolds stress tensor and the positivity of the total energy, are important topics that warrant further exploration (see [32]).

Eventually, an order upgrade could be envisaged relying on the Riemann problem solution carried in Sections 4 and 5, coupled with some higher-order methods on the treatment of non-conservative hyperbolic systems (see *e.g.*, [33]).

#### ACKNOWLEDGMENTS

All computational facilities have been provided by EDF. The authors would like to thank Thierry Gallouet and Sergey Gavriluk for useful discussions and advice.

#### FUNDING

The first author has benefited from partial support of ANRT through CIFRE contract 2023/0939.

## DATA AVAILABILITY STATEMENT

The research data associated with this article are included in the article.

## REFERENCES

- [1] M.R. Baer and J.W. Nunziato, A two-phase mixture theory for the deflagration-to-detonation transition (DDT) in reactive granular materials. *Int. J. Multiphase Flow* **12** (1986) 861–889.
- [2] C. Berthon, F. Coquel, J.-M. Hérard and M. Uhlmann, An approximate solution of the Riemann problem for a realisable second-moment turbulent closure. *Shock Waves* **11** (2002) 245–269.
- [3] C. Berthon, F. Coquel and P.G. LeFloch, Why many theories of shock waves are necessary: kinetic relations for non-conservative systems. *Proc. R. Soc. Edinburgh Sect. A: Math.* **142** (2012) 1–37.
- [4] A. Bhole, B. Nkonga, S. Gavriluk and K. Ivanova, Fluctuation splitting Riemann solver for a non-conservative modeling of shear shallow water flow. *J. Comput. Phys.* **392** (2019) 205–226.
- [5] F. Bouchut, Nonlinear Stability of Finite Volume Methods for Hyperbolic Conservation Laws: and Well-Balanced Schemes for Sources. *Frontiers in Mathematics*. Springer, Birkhäuser Basel (2004).
- [6] G. Brun, J.-M. Hérard, D. Jeandel and M. Uhlmann, An approximate Roe-type Riemann solver for a class of realizable second order closures. *Int. J. Comput. Fluid Dyn.* **13** (2000) 223–249.
- [7] C. Chalons, Path-conservative in-cell discontinuous reconstruction schemes for non conservative hyperbolic systems. *Commun. Math. Sci.* **18** (2020) 1–30.
- [8] C. Chalons and F. Coquel, A new comment on the computation of non-conservative products using Roe-type path conservative schemes. *J. Comput. Phys.* **335** (2017) 592–604.
- [9] C. Chalons and J.-F. Coulombel, Relaxation approximation of the Euler equations. *J. Math. Anal. App.* **348** (2008) 872–893.
- [10] G.-Q. Chen, C.D. Levermore and T.-P. Liu, Hyperbolic conservation laws with stiff relaxation terms and entropy. *Commun. Pure Appl. Math.* **47** (1994) 787–830.
- [11] A.J. Chorin, Numerical solution of the Navier–Stokes equations. *Math. Comput.* **22** (1968) 745–762.
- [12] F. Coquel, E. Godlewski and N. Seguin, Relaxation of fluid systems. *Math. Models Methods Appl. Sci.* **22** (2012) 1250014.
- [13] G. Dal Maso, P. Le Floch and F. Murat, Definition and weak stability of nonconservative products. *Journal de mathématiques pures et appliquées* **74** (1995) 483–548.
- [14] V. Dolejší and T. Gallouët, A numerical study of a particular non-conservative hyperbolic problem. *Comput. Fluids* **37** (2008) 1077–1091.
- [15] R. du Vachat, Realizability inequalities in turbulent flows. *Phys. Fluids* **20** (1977) 551–556.
- [16] F. Dubois, Partial Riemann problem, boundary conditions, and gas dynamics, in *Absorbing Boundaries and Layers, Domain Decomposition Methods: Applications to Large Scale Computers*. <https://hal.science/hal-00555600/document> (2001) 16.
- [17] M. Ferrand, J.-M. Hérard, T. Norddine and S. Ruget, Stable schemes for second-moment turbulent models for incompressible flows. *C. R. Méc.* **351** (2023) 337–353.
- [18] A. Forestier, J.-M. Hérard and X. Louis, A Godunov type solver for turbulent compressible flows. *C. R. Acad. Sci. Paris* **324** (1997) 919–926.
- [19] T. Gallouët, J.-M. Hérard and N. Seguin, Some recent finite volume schemes to compute Euler equations using real gas EOS. *Int. J. Numer. Methods Fluids* **39** (2002) 1073–1138.
- [20] S. Gavriluk, K. Ivanova and N. Favrie, Multi-dimensional shear shallow water flows: problems and solutions. *J. Comput. Phys.* **366** (2018) 252–280.
- [21] E. Godlewski and P.-A. Raviart, *Numerical Approximation of Hyperbolic Systems of Conservation Laws*. Vol. 118. Springer Science & Business Media (1996).
- [22] S.K. Godunov, A difference scheme for numerical solution of discontinuous solution of hydrodynamic equations. *Math. Sbornik* **47** (1959) 271–306.
- [23] J.-M. Hérard, Basic analysis of some second moment closures part I: incompressible isothermal turbulent flows. *Theor. Comput. Fluid Dyn.* **6** (1994) 213–233.
- [24] J.-M. Hérard, Basic analysis of some second moment closures part II: incompressible turbulent flows including buoyant effects. Internal EDF report HE-41/93.37A. <https://hal.science/hal-02007060/document> (1994).
- [25] S. Jin and Z. Xin, The relaxation schemes for systems of conservation laws in arbitrary space dimensions. *Commun. Pure Appl. Math.* **48** (1995) 235–276.

- [26] P.G. Le Floch, Shock Waves for Nonlinear Hyperbolic Systems in Nonconservative Form. *IMA Preprint Series* 593. <https://conservancy.umn.edu/bitstream/handle/11299/5107/593.pdf> (1989).
- [27] R. Lewandowski and B. Mohammadi, Existence and positivity results for the  $\varphi$ - $\theta$  and a modified  $k$ - $\varepsilon$  two-equation turbulence models. *Math. Models Methods Appl. Sci.* **3** (1993) 195–215.
- [28] J.L. Lumley, Computational modeling of turbulent flows. *Adv. Appl. Mech.* **18** (1979) 123–176.
- [29] M.L. Muñoz-Ruiz and C. Parés, Godunov method for nonconservative hyperbolic systems. *ESAIM: Math. Modell. Numer. Anal.* **41** (2007) 169–185.
- [30] R. Natalini, Recent Mathematical Results on Hyperbolic Relaxation Problems. *Quaderno IAC* 7. [https://www.researchgate.net/profile/Roberto-Natalini/publication/2552522\\_Recent-Mathematical-Results-on-Hyperbolic-Relaxation-Problems/links/5656e8cb08ae1ef9297b80e2/Recent-Mathematical-Results-on-Hyperbolic-Relaxation-Problems.pdf](https://www.researchgate.net/profile/Roberto-Natalini/publication/2552522_Recent-Mathematical-Results-on-Hyperbolic-Relaxation-Problems/links/5656e8cb08ae1ef9297b80e2/Recent-Mathematical-Results-on-Hyperbolic-Relaxation-Problems.pdf) (1998).
- [31] B. Nkonga and P. Chandrashekar, Exact solution for Riemann problems of the shear shallow water model. *ESAIM: Math. Modell. Numer. Anal.* **56** (2022) 1115–1150.
- [32] T. Norddine, M. Ferrand and S. Benhamadouche, Realizability-preserving time-stepping for the differential Reynolds stress turbulence models. *J. Comput. Phys.* **494** (2023) 112511.
- [33] C. Parés, Numerical methods for nonconservative hyperbolic systems: a theoretical framework. *SIAM J. Numer. Anal.* **44** (2006) 300–321.
- [34] S.B. Pope, Turbulent Flows. Cambridge University Press (2000).
- [35] P.-A. Raviart and L. Sainsaulieu, A nonconservative hyperbolic system modeling spray dynamics. Part I: solution of the Riemann problem. *Math. Models Methods Appl. Sci.* **5** (1995) 297–333.
- [36] P. Richards and S. Norris, Appropriate boundary conditions for computational wind engineering models revisited. *J. Wind Eng. Ind. Aerodyn.* **99** (2011) 257–266.
- [37] J. Rotta, Statistische theorie nichthomogener turbulenz. *Z. Phys.* **129** (1951) 547–572.
- [38] V.V. Rusanov, The calculation of the interaction of non-stationary shock waves with barriers. *Zhurnal Vychislitel'noi Matematiki i Matematicheskoi Fiziki* **1** (1961) 267–279.
- [39] L. Sainsaulieu, Contribution à la modélisation mathématique et numérique des écoulements diphasiques constitués d'un nuage de particules dans un écoulement de gaz, habilitation à diriger des recherches. Technical report, Université Paris VI (1995).
- [40] U. Schumann, Realizability of Reynolds-stress turbulence models. *Phys. Fluids* **20** (1977) 721–725.
- [41] J. Smoller, Shock Waves and Reaction–Diffusion Equations. *Grundlehren der mathematischen Wissenschaften*. Springer New York (1983).
- [42] I. Suliciu, On the thermodynamics of rate-type fluids and phase transitions. I. Rate-type fluids. *Int. J. Eng. Sci.* **36** (1998) 921–947.
- [43] R. Temam, Une méthode d'approximation de la solution des équations de Navier–Stokes. *Bull. Soc. Math. Fr.* **96** (1968) 115–152.
- [44] S. Tiwari, B. Nkonga, P. Chandrashekar and S. Gavriluk, Finite volume approximations of shear shallow water model on unstructured grids. Preprint: [https://hal.science/hal-04403870/file/SSW\\_unstructured.pdf](https://hal.science/hal-04403870/file/SSW_unstructured.pdf) (2024).
- [45] E.F. Toro, Riemann solvers and numerical methods for fluid dynamics: a practical introduction. Springer Science & Business Media (2013).
- [46] O. Troshkin, On wave properties of an incompressible turbulent fluid. *Phys. A: Stat. Mech. App.* **168** (1990) 881–899.
- [47] O. Troshkin, Nontraditional Methods in Mathematical Hydrodynamics. Vol. 144. American Mathematical Society (1995).



**Please help to maintain this journal in open access!**

This journal is currently published in open access under the Subscribe to Open model (S2O). We are thankful to our subscribers and supporters for making it possible to publish this journal in open access in the current year, free of charge for authors and readers.

Check with your library that it subscribes to the journal, or consider making a personal donation to the S2O programme by contacting [subscribers@edpsciences.org](mailto:subscribers@edpsciences.org).

More information, including a list of supporters and financial transparency reports, is available at <https://edpsciences.org/en/subscribe-to-open-s2o>.

APPENDIX A. TEST CASE 2BIS: STATIONARY CONTACT DISCONTINUITY

This test case is the same as the test case 2 in paragraph 6.2. The initial conditions, which are recalled in Table A.1, only allow a contact discontinuity for the variable  $R_{\tau\tau}$  through the LD 3-wave as it can be observed in Figure A.1. Normal velocity  $u_n$  is taken here as null. This configuration leads to a *stationary* LD 3-wave. One can observe that both Riemann solvers accurately capture the contact discontinuity with null error, whereas the Rusanov scheme diffuses as in Section 6.2 and converges at order 1/2 (see Tab. A.2).

TABLE A.1. Case 2 bis initial data.

	$u_n$	$R_{nn}$	$u_\tau$	$R_{n\tau}$	$R_{\tau\tau}$
$L$	0	0.5	1	0.1	0.5
$R$	0	0.5	1	0.1	0.8

TABLE A.2. Case 2 bis relative  $L^1$  errors and convergence rates  $\alpha$ .

	$N_c$	$u_n$		$R_{nn}$		$u_\tau$		$R_{n\tau}$		$R_{\tau\tau}$	
		Err	$\alpha$	Err	$\alpha$	Err	$\alpha$	Err	$\alpha$	Err	$\alpha$
Godunov-type	100	0		0		0		0		0	
	200	0		0		0		0		0	
	400	0		0		0		0		0	
	800	0		0		0		0		0	
	1600	0		0		0		0		0	
	3200	0		0		0		0		0	
	6400	0		0		0		0		0	
RS	100	0		0		0		0		0	
	200	0		0		0		0		0	
	400	0		0		0		0		0	
	800	0		0		0		0		0	
	1600	0		0		0		0		0	
	3200	0		0		0		0		0	
	6400	0		0		0		0		0	
Rusanov	100	0		0		0		0		$1.42 \times 10^{-2}$	
	200	0		0		0		0		$1.01 \times 10^{-2}$	0.49
	400	0		0		0		0		$7.13 \times 10^{-3}$	0.50
	800	0		0		0		0		$5.04 \times 10^{-3}$	0.50
	1600	0		0		0		0		$3.57 \times 10^{-3}$	0.50
	3200	0		0		0		0		$2.52 \times 10^{-3}$	0.50
	6400	0		0		0		0		$1.78 \times 10^{-3}$	0.50

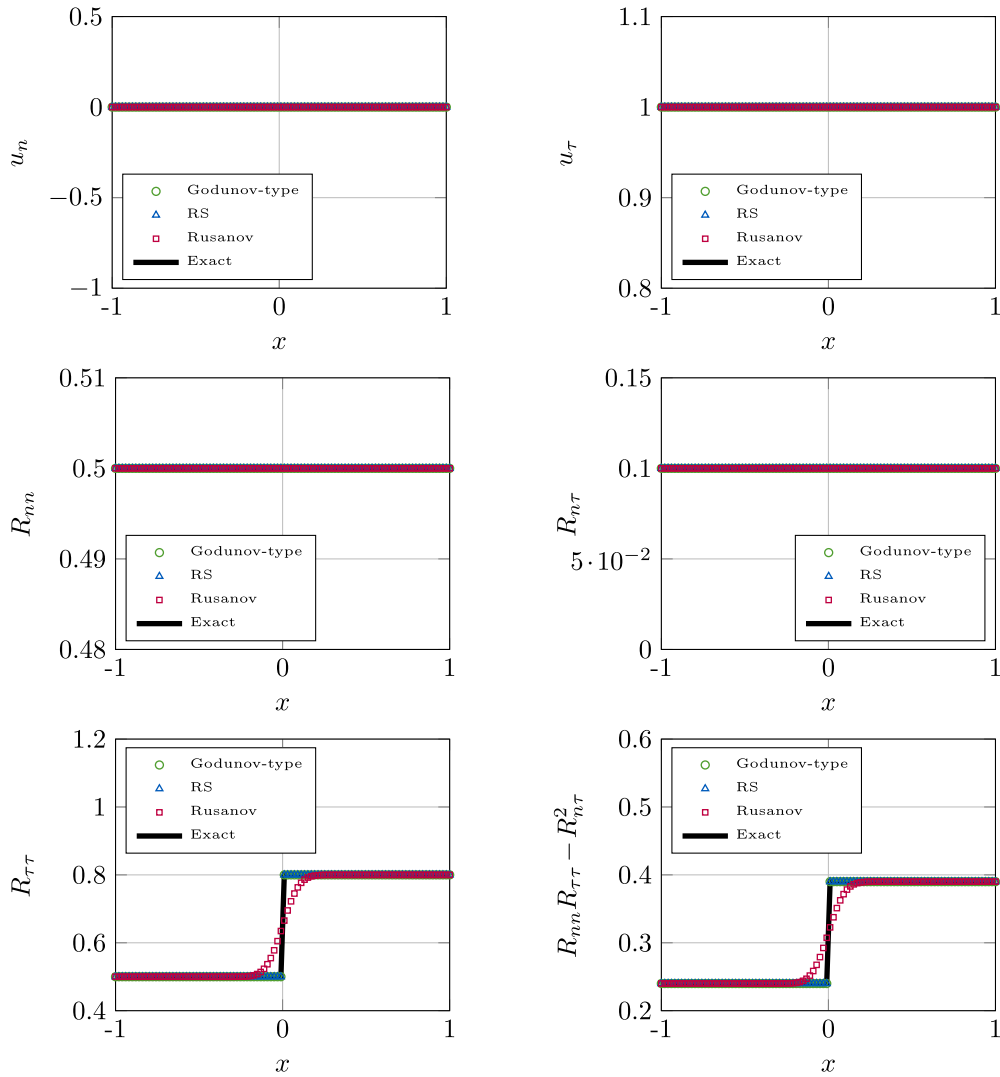


FIGURE A.1. Case 2 bis numerical solutions with  $N_c = 100$ ,  $t_f = 0.3 \frac{\mathcal{L}}{\sqrt{2R_{nn}^L}}$ .

APPENDIX B. TEST CASE 1BIS: STATIONARY 2-WAVE

This test case is analogous to test case (Sect. 6.1), with slight differences in the setup. The initial conditions, as outlined in Table B.1, permit to both GNL 1-wave and 5-wave as well as the LD 3-wave to be ghost waves, as shown in Figure B.1. In this case, the normal left velocity  $u_n^L$  is equal to  $\sqrt{R_{nn}^L}$ , such that the LD 2-wave of speed  $u_n^L - \sqrt{R_{nn}^L}$  is stationary. The Godunov-type and relaxation solvers are able to locally capture the contact discontinuity through the 2-wave with perfect accuracy, while the Rusanov scheme shows diffusion behaviour. The three schemes achieve convergence at an order of 1/2 (see Tab. B.2).

TABLE B.1. Case 1 *bis* initial data.

	$u_n$	$R_{nn}$	$u_\tau$	$R_{n\tau}$	$R_{\tau\tau}$
$L$	1	1	2	0.2	1
$R$	1	1	2	-0.2	1

TABLE B.2. Case 1 *bis* relative  $L^1$  errors and convergence rates  $\alpha$ .

	$N_c$	$u_n$		$R_{nn}$		$u_\tau$		$R_{n\tau}$		$R_{\tau\tau}$	
		Err	$\alpha$	Err	$\alpha$	Err	$\alpha$	Err	$\alpha$	Err	$\alpha$
Godunov-type	100	0				$3.40 \times 10^{-3}$		$5.00 \times 10^{-2}$		$2.73 \times 10^{-3}$	
	200	0				$2.39 \times 10^{-3}$	0.51	$3.52 \times 10^{-2}$	0.51	$1.86 \times 10^{-3}$	0.55
	400	0				$1.69 \times 10^{-3}$	0.50	$2.48 \times 10^{-2}$	0.50	$1.28 \times 10^{-3}$	0.54
	800	0				$1.19 \times 10^{-3}$	0.50	$1.75 \times 10^{-2}$	0.50	$9.06 \times 10^{-4}$	0.50
	1600	0				$8.42 \times 10^{-4}$	0.50	$1.24 \times 10^{-2}$	0.50	$6.18 \times 10^{-4}$	0.55
	3200	0				$5.96 \times 10^{-4}$	0.50	$8.76 \times 10^{-3}$	0.50	$4.39 \times 10^{-4}$	0.49
	6400	0				$4.21 \times 10^{-4}$	0.50	$6.19 \times 10^{-3}$	0.50	$3.07 \times 10^{-4}$	0.52
RS	100	0				$3.40 \times 10^{-3}$		$5.00 \times 10^{-2}$		$2.32 \times 10^{-3}$	
	200	0				$2.39 \times 10^{-3}$	0.51	$3.52 \times 10^{-2}$	0.51	$1.66 \times 10^{-3}$	0.49
	400	0				$1.69 \times 10^{-3}$	0.50	$2.48 \times 10^{-2}$	0.50	$1.18 \times 10^{-3}$	0.49
	800	0				$1.19 \times 10^{-3}$	0.50	$1.75 \times 10^{-2}$	0.50	$8.56 \times 10^{-4}$	0.47
	1600	0				$8.42 \times 10^{-4}$	0.50	$1.24 \times 10^{-2}$	0.50	$5.93 \times 10^{-4}$	0.53
	3200	0				$5.96 \times 10^{-4}$	0.50	$8.76 \times 10^{-3}$	0.50	$4.27 \times 10^{-4}$	0.48
	6400	0				$4.21 \times 10^{-4}$	0.50	$6.19 \times 10^{-3}$	0.50	$3.01 \times 10^{-4}$	0.50
Rusanov	100	0				$8.56 \times 10^{-3}$		$1.26 \times 10^{-1}$		$6.65 \times 10^{-3}$	
	200	0				$6.05 \times 10^{-3}$	0.50	$8.90 \times 10^{-2}$	0.50	$4.62 \times 10^{-3}$	0.53
	400	0				$4.27 \times 10^{-3}$	0.50	$6.29 \times 10^{-2}$	0.50	$3.21 \times 10^{-3}$	0.53
	800	0				$3.02 \times 10^{-3}$	0.50	$4.44 \times 10^{-2}$	0.50	$2.25 \times 10^{-3}$	0.51
	1600	0				$2.14 \times 10^{-3}$	0.50	$3.14 \times 10^{-2}$	0.50	$1.56 \times 10^{-3}$	0.53
	3200	0				$1.51 \times 10^{-3}$	0.50	$2.22 \times 10^{-2}$	0.50	$1.10 \times 10^{-3}$	0.50
	6400	0				$1.07 \times 10^{-3}$	0.50	$1.57 \times 10^{-2}$	0.50	$7.73 \times 10^{-4}$	0.51

APPENDIX C. VANISHING VISCOSITY METHOD FOR  $u_\tau$  AND  $R_{\tau\tau}$  IN THE NON-TURBULENT REGION

In this appendix, we introduce a viscous perturbation of system (3.19), using viscous terms which are present in the original system (1.1):

$$\begin{cases} \partial_t u_\tau + u_n \partial_n u_\tau - \nu_0 \epsilon_0 \partial_{nn} u_\tau = 0, \\ \partial_t R_{\tau\tau} + u_n \partial_n R_{\tau\tau} - \nu_0 \epsilon_0 \partial_{nn} R_{\tau\tau} = 0, \end{cases} \tag{C.1}$$

with  $\epsilon_0 \in [0, 1]$  and  $\nu_0 > 0$  the kinematic viscosity.

We consider a regular function  $\tilde{f}_\epsilon(\frac{x}{\epsilon}) = \tilde{f}_\epsilon(\xi)$ . Owing to (3.21), it will be a solution of (C.1) if  $\tilde{f}_\epsilon$  satisfies:

$$\epsilon_0 \partial_{nn} \tilde{f}_\epsilon = 0 \quad \forall \epsilon_0 > 0. \tag{C.2}$$

This gives  $\partial_{nn} \tilde{f}_\epsilon = 0$ , thus  $\partial_n \tilde{f}_\epsilon = a(t)$ , which gives:

$$\frac{1}{\epsilon} \tilde{f}'_\epsilon(\xi) = a(t) \tag{C.3}$$

and eventually:

$$\tilde{f}'_\epsilon(\xi) = t \times a(t) = A_0, \tag{C.4}$$

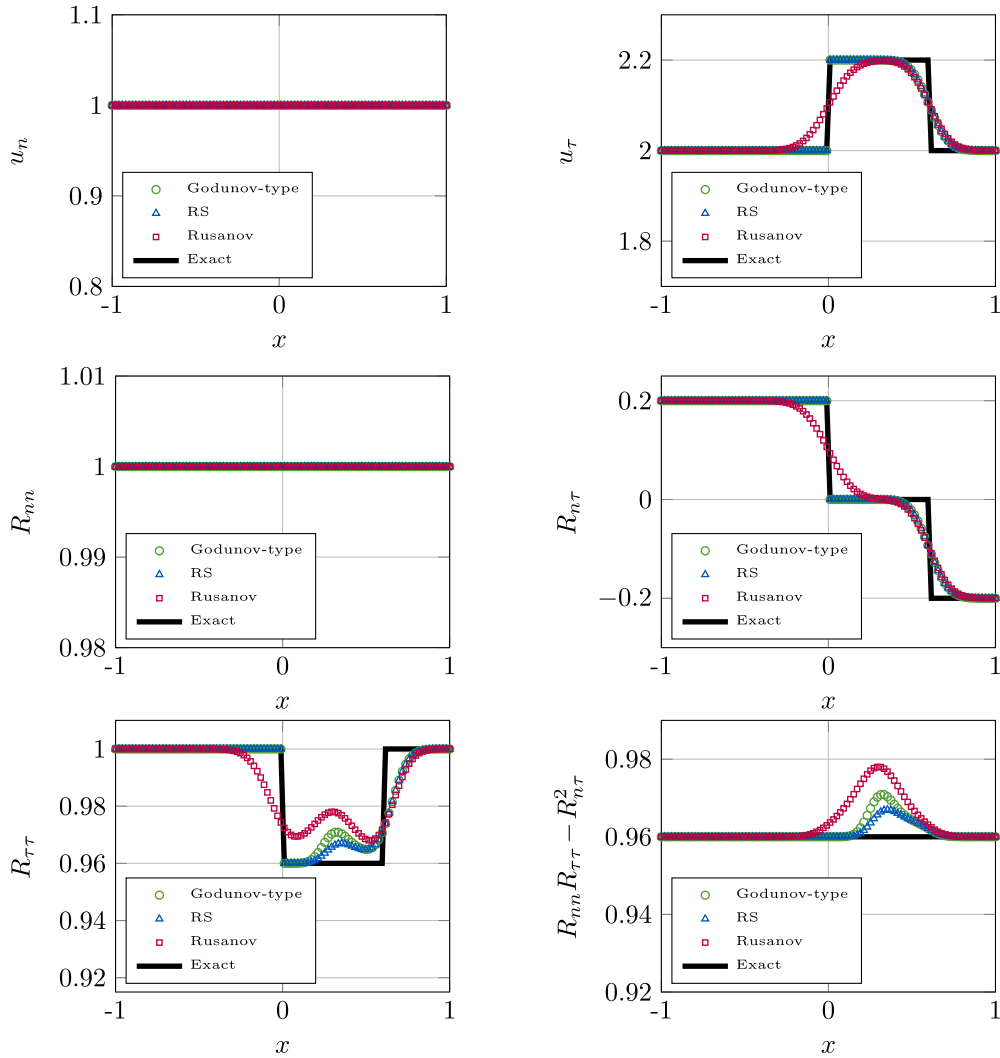


FIGURE B.1. Case 1 bis numerical solutions with  $N_c = 100$ ,  $t_f = 0.3 \frac{\mathcal{L}}{\sqrt{2R_{nn}^L}}$ .

because  $\xi$  and  $t$  are independent variables. Hence:

$$\tilde{f}_\epsilon(\xi) = A_0\xi + B_0, \tag{C.5}$$

where:

$$\begin{cases} \tilde{f}_\epsilon(\xi^-) = A_0\xi^- + B_0, \\ \tilde{f}_\epsilon(\xi^+) = A_0\xi^+ + B_0. \end{cases} \tag{C.6}$$

As soon as  $\xi^- \neq \xi^+$ , the solution of (C.1) is uniquely defined by the linear connection of the states  $\xi^-$  and  $\xi^+$ . By moving to the limit in (C.1), we obtain:

$$\tilde{f}(\xi) := \lim_{\epsilon \rightarrow 0^+} \tilde{f}_\epsilon(\xi) = A_0\xi + B_0. \tag{C.7}$$

TABLE C.1. Case 4 bis initial data.

	$u_n$	$R_{nn}$	$u_\tau$	$R_{n\tau}$	$R_{\tau\tau}$
$L$	$-1.01 \times \sqrt{2}$	1	1	-0.1	0.5
$R$	$1.01 \times \sqrt{2}$	1	1	0.1	0.5

TABLE C.2. Case 4 bis relative  $L^1$  errors and convergence rates  $\alpha$ .

	$N_c$	$u_n$		$R_{nn}$		$u_\tau$		$R_{n\tau}$		$R_{\tau\tau}$	
		Err	$\alpha$	Err	$\alpha$	Err	$\alpha$	Err	$\alpha$	Err	$\alpha$
Godunov-type	100	$3.74 \times 10^{-2}$		$6.14 \times 10^{-2}$		$3.60 \times 10^{-3}$		$5.42 \times 10^{-2}$		$7.01 \times 10^{-4}$	
	200	$2.32 \times 10^{-2}$	0.69	$3.68 \times 10^{-2}$	0.74	$2.41 \times 10^{-3}$	0.58	$3.12 \times 10^{-2}$	0.80	$4.16 \times 10^{-4}$	0.76
	400	$1.40 \times 10^{-2}$	0.72	$2.18 \times 10^{-2}$	0.76	$1.66 \times 10^{-3}$	0.54	$1.85 \times 10^{-2}$	0.75	$2.60 \times 10^{-4}$	0.68
	800	$8.29 \times 10^{-3}$	0.76	$1.27 \times 10^{-2}$	0.78	$1.17 \times 10^{-3}$	0.50	$1.12 \times 10^{-2}$	0.73	$1.75 \times 10^{-4}$	0.57
	1600	$4.82 \times 10^{-3}$	0.78	$7.29 \times 10^{-3}$	0.80	$8.33 \times 10^{-4}$	0.49	$6.85 \times 10^{-3}$	0.70	$1.22 \times 10^{-4}$	0.53
	3200	$2.77 \times 10^{-3}$	0.80	$4.14 \times 10^{-3}$	0.82	$6.10 \times 10^{-4}$	0.45	$4.26 \times 10^{-3}$	0.68	$8.54 \times 10^{-5}$	0.51
	6400	$1.57 \times 10^{-3}$	0.82	$2.32 \times 10^{-3}$	0.83	$4.73 \times 10^{-4}$	0.37	$2.69 \times 10^{-3}$	0.66	$6.02 \times 10^{-5}$	0.50
RS	100	$3.44 \times 10^{-2}$		$6.34 \times 10^{-2}$		$4.70 \times 10^{-3}$		$6.80 \times 10^{-2}$		$1.28 \times 10^{-3}$	
	200	$2.19 \times 10^{-2}$	0.65	$3.74 \times 10^{-2}$	0.76	$3.07 \times 10^{-3}$	0.61	$4.34 \times 10^{-2}$	0.65	$8.91 \times 10^{-4}$	0.52
	400	$1.35 \times 10^{-2}$	0.70	$2.20 \times 10^{-2}$	0.77	$2.19 \times 10^{-3}$	0.49	$2.75 \times 10^{-2}$	0.66	$6.14 \times 10^{-4}$	0.54
	800	$8.08 \times 10^{-3}$	0.74	$1.27 \times 10^{-2}$	0.79	$1.59 \times 10^{-3}$	0.46	$1.72 \times 10^{-2}$	0.68	$4.19 \times 10^{-4}$	0.55
	1600	$4.73 \times 10^{-3}$	0.77	$7.29 \times 10^{-3}$	0.80	$1.17 \times 10^{-3}$	0.45	$1.07 \times 10^{-2}$	0.69	$2.84 \times 10^{-4}$	0.56
	3200	$2.72 \times 10^{-3}$	0.80	$4.12 \times 10^{-3}$	0.82	$8.63 \times 10^{-4}$	0.44	$6.62 \times 10^{-3}$	0.69	$1.93 \times 10^{-4}$	0.56
	6400	$1.55 \times 10^{-3}$	0.81	$2.31 \times 10^{-3}$	0.84	$6.44 \times 10^{-4}$	0.42	$4.13 \times 10^{-3}$	0.68	$1.32 \times 10^{-4}$	0.55
Rusanov	100	$3.49 \times 10^{-2}$		$6.83 \times 10^{-2}$		$1.16 \times 10^{-2}$		$8.82 \times 10^{-2}$		$4.51 \times 10^{-3}$	
	200	$2.16 \times 10^{-2}$	0.70	$3.94 \times 10^{-2}$	0.79	$8.23 \times 10^{-3}$	0.49	$6.21 \times 10^{-2}$	0.51	$3.44 \times 10^{-3}$	0.39
	400	$1.31 \times 10^{-2}$	0.72	$2.27 \times 10^{-2}$	0.79	$5.78 \times 10^{-3}$	0.51	$4.30 \times 10^{-2}$	0.53	$2.57 \times 10^{-3}$	0.42
	800	$7.75 \times 10^{-3}$	0.75	$1.30 \times 10^{-2}$	0.80	$4.02 \times 10^{-3}$	0.53	$2.92 \times 10^{-2}$	0.56	$1.88 \times 10^{-3}$	0.45
	1600	$4.52 \times 10^{-3}$	0.78	$7.38 \times 10^{-3}$	0.82	$2.77 \times 10^{-3}$	0.54	$1.95 \times 10^{-2}$	0.58	$1.36 \times 10^{-3}$	0.46
	3200	$2.60 \times 10^{-3}$	0.80	$4.14 \times 10^{-3}$	0.83	$1.90 \times 10^{-3}$	0.54	$1.30 \times 10^{-2}$	0.59	$9.82 \times 10^{-4}$	0.48
	6400	$1.48 \times 10^{-3}$	0.81	$2.31 \times 10^{-3}$	0.84	$1.48 \times 10^{-3}$	0.36	$8.61 \times 10^{-3}$	0.59	$7.05 \times 10^{-4}$	0.48

Hence, a solution for  $u_\tau$  and  $R_{\tau\tau}$  in (3.19) is the linear connection between the states  $\mathbf{w}^-$  and  $\mathbf{w}^+$  for  $u_n^- < \frac{x}{t} < u_n^+$ :

$$\begin{cases} \tilde{u}_\tau\left(\frac{x}{t}\right) = \frac{1}{u_n^+ - u_n^-} \left( (u_\tau^+ - u_\tau^-) \frac{x}{t} + u_n^+ u_\tau^- - u_n^- u_\tau^+ \right), \\ \tilde{R}_{\tau\tau}\left(\frac{x}{t}\right) = \frac{1}{u_n^+ - u_n^-} \left( (R_{\tau\tau}^+ - R_{\tau\tau}^-) \frac{x}{t} + u_n^+ R_{\tau\tau}^- - u_n^- R_{\tau\tau}^+ \right). \end{cases} \tag{C.8}$$

**C.1. Test case 4bis: wall boundary flow**

This test case is quite similar to test case 6.4, the only difference being that its initial conditions recalled in Table C.1 violate the existence and uniqueness condition (2.9) and strictly introduce a non-turbulent zone at the center  $x = 0$  (see Fig. C.1). This test case may be interpreted as a mirror state wall boundary condition where  $u_n$ ,  $R_{nn}$  and  $R_{n\tau}$  are null at  $x = 0$ .

For both Godunov-type and RS schemes, we refer to Proposition 3.1 for the implementation of the interface Riemann solver considering variables  $u_n$ ,  $R_{nn}$  and  $R_{n\tau}$ , when condition (2.9) is breached at a given interface. Meanwhile, we consider the relation (C.8) proposed in Appendix C for the variables  $u_\tau$  and  $R_{\tau\tau}$ .

The errors and convergence rates are presented in Table C.2 and are almost similar to the limit case ones presented in paragraph 6.4, Table 8.

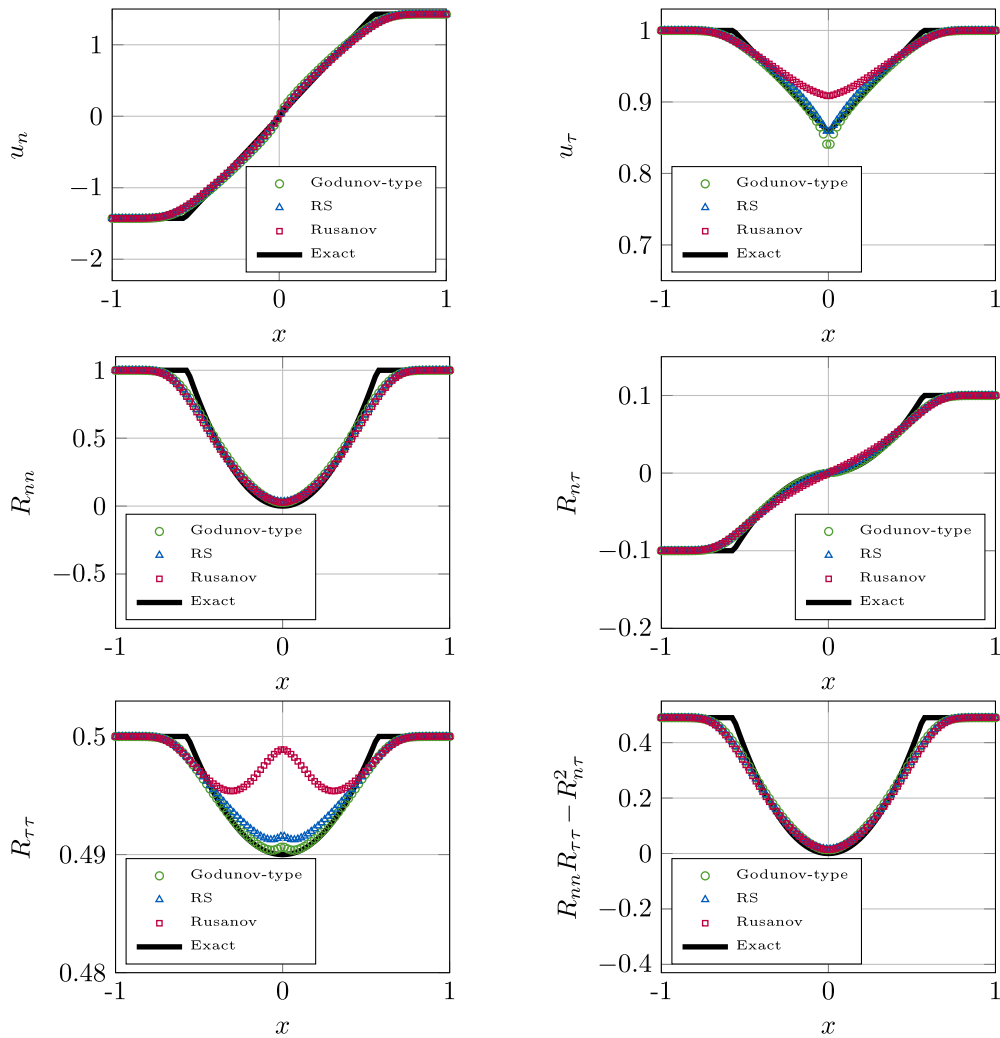


FIGURE C.1. Case 4 bis numerical solutions with  $N_c = 100$ ,  $t_f = 0.2 \frac{L}{\sqrt{R_{nn}^L}}$ .

**C.2. Test case 5: occurrence of a non-turbulent region**

In this case, initial conditions, written in Table C.3, are such that (2.9) is violated. The numerical solutions associated to the three schemes are plotted in Figure C.2.

For the variables  $u_n$  and  $R_{nn}$ , the rate of convergence reported in Table C.4 is still approximately 0.8. The accuracy is the same for all three schemes considering these variables. For  $R_{n\tau}$ , we observe an order of convergence equal to 0.7 for RS and Godunov-type schemes, which provide similar accuracies.

For the variables  $u_\tau$  and  $R_{\tau\tau}$ , the convergence rates tend to decrease when the mesh is refined, hence the numerical solutions do not seem to converge to solution (C.8) for these two variables.

TABLE C.3. Case 5 initial data.

	$u_n$	$R_{nn}$	$u_\tau$	$R_{n\tau}$	$R_{\tau\tau}$
$L$	$-\sqrt{2}$	1	1	-0.1	0.5
$R$	$1.5 \times \sqrt{2}$	1	1	0.1	0.5

TABLE C.4. Case 5 relative  $L^1$  errors and convergence rates  $\alpha$ .

	$N_c$	$u_n$		$R_{nn}$		$u_\tau$		$R_{n\tau}$		$R_{\tau\tau}$	
		Err	$\alpha$	Err	$\alpha$	Err	$\alpha$	Err	$\alpha$	Err	$\alpha$
Godunov-type	100	$3.39 \times 10^{-2}$		$7.37 \times 10^{-2}$		$6.10 \times 10^{-3}$		$8.18 \times 10^{-2}$		$1.12 \times 10^{-3}$	
	200	$2.14 \times 10^{-2}$	0.66	$4.46 \times 10^{-2}$	0.72	$4.38 \times 10^{-3}$	0.48	$5.18 \times 10^{-2}$	0.66	$7.58 \times 10^{-4}$	0.57
	400	$1.33 \times 10^{-2}$	0.69	$2.65 \times 10^{-2}$	0.75	$3.17 \times 10^{-3}$	0.47	$3.23 \times 10^{-2}$	0.68	$5.13 \times 10^{-4}$	0.56
	800	$8.14 \times 10^{-3}$	0.71	$1.55 \times 10^{-2}$	0.77	$2.35 \times 10^{-3}$	0.44	$2.01 \times 10^{-2}$	0.69	$3.50 \times 10^{-4}$	0.55
	1600	$4.90 \times 10^{-3}$	0.73	$8.97 \times 10^{-3}$	0.79	$1.78 \times 10^{-3}$	0.40	$1.23 \times 10^{-2}$	0.70	$2.42 \times 10^{-4}$	0.53
	3200	$2.90 \times 10^{-3}$	0.76	$5.12 \times 10^{-3}$	0.81	$1.40 \times 10^{-3}$	0.35	$7.52 \times 10^{-3}$	0.71	$1.71 \times 10^{-4}$	0.50
	6400	$1.69 \times 10^{-3}$	0.78	$2.88 \times 10^{-3}$	0.83	$1.14 \times 10^{-3}$	0.29	$4.59 \times 10^{-3}$	0.71	$1.25 \times 10^{-4}$	0.45
	12800	$9.70 \times 10^{-4}$	0.80	$1.61 \times 10^{-3}$	0.84	$9.66 \times 10^{-4}$	0.24	$2.81 \times 10^{-3}$	0.71	$9.57 \times 10^{-5}$	0.39
RS	100	$3.09 \times 10^{-2}$		$7.36 \times 10^{-2}$		$5.79 \times 10^{-3}$		$7.93 \times 10^{-2}$		$1.07 \times 10^{-3}$	
	200	$2.00 \times 10^{-2}$	0.63	$4.45 \times 10^{-2}$	0.73	$4.18 \times 10^{-3}$	0.47	$5.00 \times 10^{-2}$	0.67	$7.27 \times 10^{-4}$	0.56
	400	$1.27 \times 10^{-2}$	0.66	$2.64 \times 10^{-2}$	0.75	$3.01 \times 10^{-3}$	0.47	$3.10 \times 10^{-2}$	0.69	$4.95 \times 10^{-4}$	0.55
	800	$7.86 \times 10^{-3}$	0.69	$1.55 \times 10^{-2}$	0.77	$2.21 \times 10^{-3}$	0.44	$1.92 \times 10^{-2}$	0.70	$3.42 \times 10^{-4}$	0.53
	1600	$4.77 \times 10^{-3}$	0.72	$8.94 \times 10^{-3}$	0.79	$1.67 \times 10^{-3}$	0.41	$1.17 \times 10^{-2}$	0.71	$2.41 \times 10^{-4}$	0.51
	3200	$2.84 \times 10^{-3}$	0.75	$5.10 \times 10^{-3}$	0.81	$1.30 \times 10^{-3}$	0.36	$7.06 \times 10^{-3}$	0.73	$1.77 \times 10^{-4}$	0.44
	6400	$1.66 \times 10^{-3}$	0.77	$2.88 \times 10^{-3}$	0.83	$1.06 \times 10^{-3}$	0.29	$4.28 \times 10^{-3}$	0.72	$1.36 \times 10^{-4}$	0.38
	12800	$9.54 \times 10^{-4}$	0.80	$1.61 \times 10^{-3}$	0.84	$9.03 \times 10^{-4}$	0.24	$2.65 \times 10^{-3}$	0.69	$1.09 \times 10^{-4}$	0.32
Rusanov	100	$3.22 \times 10^{-2}$		$8.39 \times 10^{-2}$		$1.94 \times 10^{-2}$		$1.19 \times 10^{-1}$		$6.13 \times 10^{-3}$	
	200	$2.00 \times 10^{-2}$	0.69	$4.83 \times 10^{-2}$	0.80	$1.53 \times 10^{-2}$	0.34	$8.74 \times 10^{-2}$	0.45	$5.09 \times 10^{-3}$	0.27
	400	$1.23 \times 10^{-2}$	0.69	$2.76 \times 10^{-2}$	0.80	$1.21 \times 10^{-2}$	0.35	$6.21 \times 10^{-2}$	0.49	$4.18 \times 10^{-3}$	0.28
	800	$7.55 \times 10^{-3}$	0.71	$1.58 \times 10^{-2}$	0.80	$9.56 \times 10^{-3}$	0.34	$4.33 \times 10^{-2}$	0.52	$3.45 \times 10^{-3}$	0.28
	1600	$4.54 \times 10^{-3}$	0.73	$9.00 \times 10^{-3}$	0.82	$7.66 \times 10^{-3}$	0.32	$2.96 \times 10^{-2}$	0.55	$2.88 \times 10^{-3}$	0.26
	3200	$2.69 \times 10^{-3}$	0.76	$5.08 \times 10^{-3}$	0.83	$6.25 \times 10^{-3}$	0.29	$2.01 \times 10^{-2}$	0.56	$2.44 \times 10^{-3}$	0.24
	6400	$1.57 \times 10^{-3}$	0.78	$2.84 \times 10^{-3}$	0.84	$5.21 \times 10^{-3}$	0.26	$1.35 \times 10^{-2}$	0.57	$2.12 \times 10^{-3}$	0.20
	12800	$9.03 \times 10^{-4}$	0.80	$1.58 \times 10^{-3}$	0.85	$4.48 \times 10^{-3}$	0.22	$9.15 \times 10^{-3}$	0.57	$1.89 \times 10^{-3}$	0.17

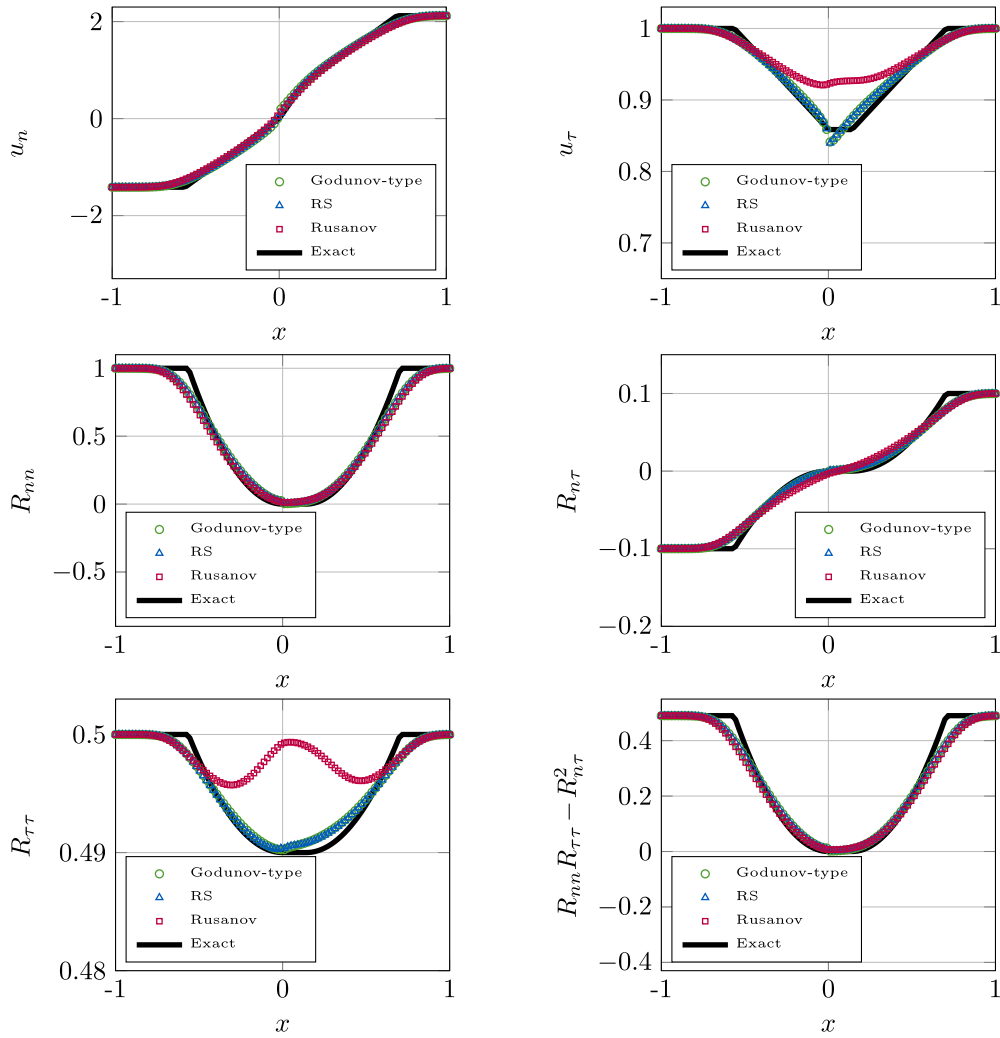


FIGURE C.2. Case 5 numerical solutions with  $N_c = 100$ ,  $t_f = 0.2 \frac{\mathcal{L}}{\sqrt{R_{nn}^L}}$ .

APPENDIX D. TEST CASE 6: INITIAL PARTIAL LAMINAR FLOW

In this test case, we use exactly zero values for  $R_{nn}^L$  and  $R_{nn}^R$  and proceed to a symmetric double rarefaction  $u_n^L = -u_n^R < 0$  as recalled in Table D.1.

Let us consider  $R_{nn}^L = R_{nn}^R = 0$ . Based on the same principle as the one detailed in Section 3, this leads to a double rarefaction configuration depicted in Figure D.1, where  $R_{nn}$  remains null everywhere.

- For realisability considerations, we have in the whole half-plane  $(x, t > 0)$ :

$$R_{nn}\left(\frac{x}{t}\right) = R_{n\nu}\left(\frac{x}{t}\right) = 0. \tag{D.1}$$

- For  $\frac{x}{t} < u_n^L$ ,  $\tilde{w}\left(\frac{x}{t}\right) = w^L$ .
- For  $\frac{x}{t} > u_n^R$ ,  $\tilde{w}\left(\frac{x}{t}\right) = \tilde{w}^R$ .
- For  $u_n^L < \frac{x}{t} < u_n^R$ , we can proceed as in Section 3:

$$\tilde{u}_n\left(\frac{x}{t}\right) = \frac{x}{t}. \tag{D.2}$$

TABLE D.1. Test case 6 initial data.

	$u_n$	$R_{nn}$	$u_\tau$	$R_{n\tau}$	$R_{\tau\tau}$
$L$	-1	0	2	0	1
$R$	1	0	1	0	0.5

There is no unique solution for  $u_\tau$  and  $R_{\tau\tau}$  as in Section 3. We propose the linear connexion between the left and right states arising from the vanishing viscosity method (see Appendix C):

$$\begin{cases} \tilde{u}_\tau\left(\frac{x}{t}\right) = \frac{1}{u_n^R - u_n^L} \left( (u_\tau^R - u_\tau^L) \frac{x}{t} + u_n^R u_\tau^L - u_n^L u_\tau^R \right), \\ \tilde{R}_{\tau\tau}\left(\frac{x}{t}\right) = \frac{1}{u_n^R - u_n^L} \left( (R_{\tau\tau}^R - R_{\tau\tau}^L) \frac{x}{t} + u_n^R R_{\tau\tau}^L - u_n^L R_{\tau\tau}^R \right). \end{cases} \tag{D.3}$$

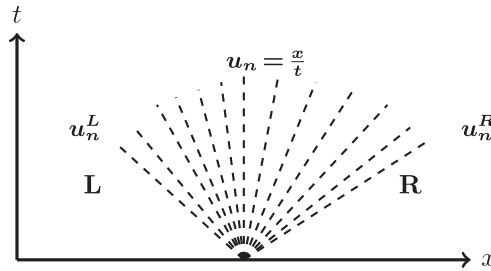


FIGURE D.1. Initial laminar case with  $u_n^R - u_n^L > 0$ .

In Table D.2 one can observe that the error for  $R_{nn}$  and  $R_{n\tau}$  remains null regardless of the mesh size. Indeed in this configuration  $R_{nn}$  is also equal to zero in the intermediate state and leads  $R_{n\tau}$  to be null for realizability consideration. This property is well captured by the three schemes as it can be seen in Figure D.2.

The variable  $u_n$ , which follows a Burgers equation in a rarefaction configuration in this case, converges at an order close to 1, similarly to the case in Appendix C.2.

Moreover, we recall that there is no unique solution for variables  $u_\tau$  and  $R_{\tau\tau}$  in the case where  $R_{nn}$  remains null everywhere. However the linear connection between the left and right states arising from the vanishing viscosity method as done in Appendix C leads here to a convergence towards the proposed solution, also at an order close to 1 for all schemes.

TABLE D.2. Case 6 relative  $L^1$  errors and convergence rates  $\alpha$ .

	$N_c$	$u_n$		$R_{nn}$		$u_\tau$		$R_{n\tau}$		$R_{\tau\tau}$	
		Err	$\alpha$	Err	$\alpha$	Err	$\alpha$	Err	$\alpha$	Err	$\alpha$
Godunov-type	100	$2.71 \times 10^{-2}$		0		$7.70 \times 10^{-3}$		0		$7.70 \times 10^{-3}$	
	200	$1.65 \times 10^{-2}$	0.72	0		$4.68 \times 10^{-3}$	0.72	0		$4.68 \times 10^{-3}$	0.72
	400	$9.89 \times 10^{-3}$	0.74	0		$2.80 \times 10^{-3}$	0.74	0		$2.80 \times 10^{-3}$	0.74
	800	$5.81 \times 10^{-3}$	0.77	0		$1.65 \times 10^{-3}$	0.77	0		$1.65 \times 10^{-3}$	0.77
	1600	$3.36 \times 10^{-3}$	0.79	0		$9.52 \times 10^{-4}$	0.79	0		$9.52 \times 10^{-4}$	0.79
	3200	$1.91 \times 10^{-3}$	0.81	0		$5.42 \times 10^{-4}$	0.81	0		$5.42 \times 10^{-4}$	0.81
	6400	$1.08 \times 10^{-3}$	0.83	0		$3.05 \times 10^{-4}$	0.83	0		$3.05 \times 10^{-4}$	0.83
RS	100	$2.71 \times 10^{-2}$		0		$7.70 \times 10^{-3}$		0		$7.70 \times 10^{-3}$	
	200	$1.65 \times 10^{-2}$	0.72	0		$4.68 \times 10^{-3}$	0.72	0		$4.68 \times 10^{-3}$	0.72
	400	$9.89 \times 10^{-3}$	0.74	0		$2.80 \times 10^{-3}$	0.74	0		$2.80 \times 10^{-3}$	0.74
	800	$5.81 \times 10^{-3}$	0.77	0		$1.65 \times 10^{-3}$	0.77	0		$1.65 \times 10^{-3}$	0.77
	1600	$3.36 \times 10^{-3}$	0.79	0		$9.52 \times 10^{-4}$	0.79	0		$9.52 \times 10^{-4}$	0.79
	3200	$1.91 \times 10^{-3}$	0.81	0		$5.42 \times 10^{-4}$	0.81	0		$5.42 \times 10^{-4}$	0.81
	6400	$1.08 \times 10^{-3}$	0.83	0		$3.05 \times 10^{-4}$	0.83	0		$3.05 \times 10^{-4}$	0.83
Rusanov	100	$3.01 \times 10^{-2}$		0		$8.55 \times 10^{-3}$		0		$8.55 \times 10^{-3}$	
	200	$1.71 \times 10^{-2}$	0.81	0		$4.86 \times 10^{-3}$	0.81	0		$4.86 \times 10^{-3}$	0.81
	400	$9.81 \times 10^{-3}$	0.80	0		$2.78 \times 10^{-3}$	0.81	0		$2.78 \times 10^{-3}$	0.81
	800	$5.60 \times 10^{-3}$	0.81	0		$1.59 \times 10^{-3}$	0.81	0		$1.59 \times 10^{-3}$	0.81
	1600	$3.18 \times 10^{-3}$	0.82	0		$9.01 \times 10^{-4}$	0.82	0		$9.01 \times 10^{-4}$	0.82
	3200	$1.79 \times 10^{-3}$	0.83	0		$5.08 \times 10^{-4}$	0.83	0		$5.08 \times 10^{-4}$	0.83
	6400	$1.00 \times 10^{-3}$	0.84	0		$2.83 \times 10^{-4}$	0.84	0		$2.83 \times 10^{-4}$	0.84

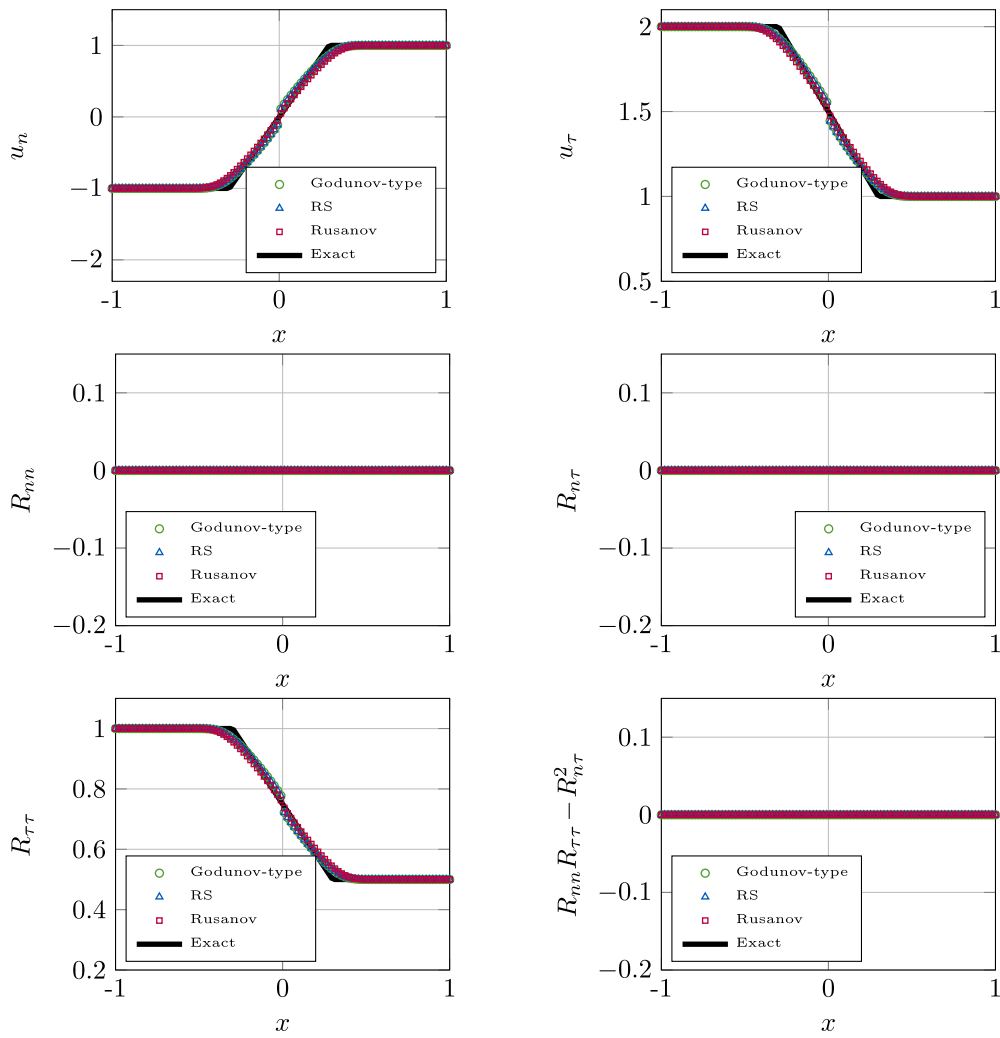


FIGURE D.2. Case 6 numerical solutions with  $N_c = 100$ ,  $t_f = 0.3 \frac{2\mathcal{L}}{|u_n^R - u_n^L|}$ .

APPENDIX E. TEST CASE 7: INITIAL PARTIAL LAMINAR-TURBULENT CONNECTION

In this case, we consider a situation where  $R_{nn}^L > 0$  and  $R_{nn}^R = 0$ . The values of the remaining variables of the right state, recalled in Table E.1, are such that  $\mathbf{w}^R = \mathbf{w}^1$  where  $\mathbf{w}^1$  is the state obtained using the Riemann invariants of the 1-rarefaction starting from the left state  $\mathbf{w}^L$ .

Moreover,  $u_n^L$  is taken such that  $u_n^L - \sqrt{2R_{nn}^L} = 0$ , allowing the beginning of the 1-rarefaction to be stationary. One can observe in Figure E.1 that the solution is perfectly captured by the Godunov-type and relaxation schemes to the left of the 1-rarefaction wave.

The errors and order of convergence are recalled in Table E.2 where one observes convergence rates close to 1, which is expected.

TABLE E.1. Case 7 initial data.

	$u_n$	$R_{nn}$	$u_\tau$	$R_{n\tau}$	$R_{\tau\tau}$
$L$	$\sqrt{2}$	1	2	0.5	1
$R$	$2\sqrt{2}$	0	$2 + \frac{1}{2\sqrt{2}}$	0	0.75

TABLE E.2. Case 7 relative  $L^1$  errors and convergence rates  $\alpha$ .

	$N_c$	$u_n$		$R_{nn}$		$u_\tau$		$R_{n\tau}$		$R_{\tau\tau}$	
		Err	$\alpha$	Err	$\alpha$	Err	$\alpha$	Err	$\alpha$	Err	$\alpha$
Godunov-type	100	$7.74 \times 10^{-3}$		$1.95 \times 10^{-2}$		$3.35 \times 10^{-3}$		$1.95 \times 10^{-2}$		$3.12 \times 10^{-3}$	
	200	$4.65 \times 10^{-3}$	0.73	$1.17 \times 10^{-2}$	0.74	$2.01 \times 10^{-3}$	0.73	$1.17 \times 10^{-2}$	0.74	$1.87 \times 10^{-3}$	0.74
	400	$2.80 \times 10^{-3}$	0.73	$6.81 \times 10^{-3}$	0.78	$1.21 \times 10^{-3}$	0.73	$6.81 \times 10^{-3}$	0.78	$1.09 \times 10^{-3}$	0.78
	800	$1.68 \times 10^{-3}$	0.74	$3.89 \times 10^{-3}$	0.81	$7.27 \times 10^{-4}$	0.74	$3.89 \times 10^{-3}$	0.81	$6.21 \times 10^{-4}$	0.81
	1600	$1.01 \times 10^{-3}$	0.74	$2.19 \times 10^{-3}$	0.83	$4.35 \times 10^{-4}$	0.74	$2.19 \times 10^{-3}$	0.83	$3.49 \times 10^{-4}$	0.83
	3200	$5.99 \times 10^{-4}$	0.75	$1.21 \times 10^{-3}$	0.85	$2.59 \times 10^{-4}$	0.75	$1.21 \times 10^{-3}$	0.85	$1.94 \times 10^{-4}$	0.85
	6400	$3.54 \times 10^{-4}$	0.76	$6.67 \times 10^{-4}$	0.86	$1.53 \times 10^{-4}$	0.76	$6.67 \times 10^{-4}$	0.86	$1.07 \times 10^{-4}$	0.86
RS	100	$7.79 \times 10^{-3}$		$1.97 \times 10^{-2}$		$3.49 \times 10^{-3}$		$2.04 \times 10^{-2}$		$3.47 \times 10^{-3}$	
	200	$4.68 \times 10^{-3}$	0.73	$1.18 \times 10^{-2}$	0.74	$2.15 \times 10^{-3}$	0.70	$1.24 \times 10^{-2}$	0.72	$2.14 \times 10^{-3}$	0.69
	400	$2.82 \times 10^{-3}$	0.73	$6.86 \times 10^{-3}$	0.78	$1.36 \times 10^{-3}$	0.67	$7.41 \times 10^{-3}$	0.74	$1.33 \times 10^{-3}$	0.69
	800	$1.69 \times 10^{-3}$	0.74	$3.91 \times 10^{-3}$	0.81	$8.67 \times 10^{-4}$	0.65	$4.43 \times 10^{-3}$	0.74	$8.31 \times 10^{-4}$	0.68
	1600	$1.01 \times 10^{-3}$	0.74	$2.20 \times 10^{-3}$	0.83	$5.63 \times 10^{-4}$	0.62	$2.66 \times 10^{-3}$	0.74	$5.24 \times 10^{-4}$	0.66
	3200	$6.00 \times 10^{-4}$	0.75	$1.22 \times 10^{-3}$	0.85	$3.69 \times 10^{-4}$	0.61	$1.60 \times 10^{-3}$	0.73	$3.33 \times 10^{-4}$	0.65
	6400	$3.54 \times 10^{-4}$	0.76	$6.71 \times 10^{-4}$	0.86	$2.43 \times 10^{-4}$	0.60	$9.75 \times 10^{-4}$	0.72	$2.13 \times 10^{-4}$	0.65
Rusanov	100	$1.53 \times 10^{-2}$		$5.06 \times 10^{-2}$		$6.62 \times 10^{-3}$		$5.06 \times 10^{-2}$		$8.08 \times 10^{-3}$	
	200	$9.60 \times 10^{-3}$	0.67	$3.06 \times 10^{-2}$	0.73	$4.15 \times 10^{-3}$	0.67	$3.06 \times 10^{-2}$	0.73	$4.89 \times 10^{-3}$	0.72
	400	$5.99 \times 10^{-3}$	0.68	$1.83 \times 10^{-2}$	0.74	$2.59 \times 10^{-3}$	0.68	$1.83 \times 10^{-2}$	0.74	$2.92 \times 10^{-3}$	0.74
	800	$3.69 \times 10^{-3}$	0.70	$1.07 \times 10^{-2}$	0.77	$1.59 \times 10^{-3}$	0.70	$1.07 \times 10^{-2}$	0.77	$1.72 \times 10^{-3}$	0.77
	1600	$2.23 \times 10^{-3}$	0.72	$6.22 \times 10^{-3}$	0.79	$9.67 \times 10^{-4}$	0.72	$6.22 \times 10^{-3}$	0.79	$9.95 \times 10^{-4}$	0.79
	3200	$1.33 \times 10^{-3}$	0.75	$3.56 \times 10^{-3}$	0.81	$5.77 \times 10^{-4}$	0.75	$3.56 \times 10^{-3}$	0.81	$5.68 \times 10^{-4}$	0.81
	6400	$7.84 \times 10^{-4}$	0.77	$2.01 \times 10^{-3}$	0.82	$3.39 \times 10^{-4}$	0.77	$2.01 \times 10^{-3}$	0.82	$3.21 \times 10^{-4}$	0.82

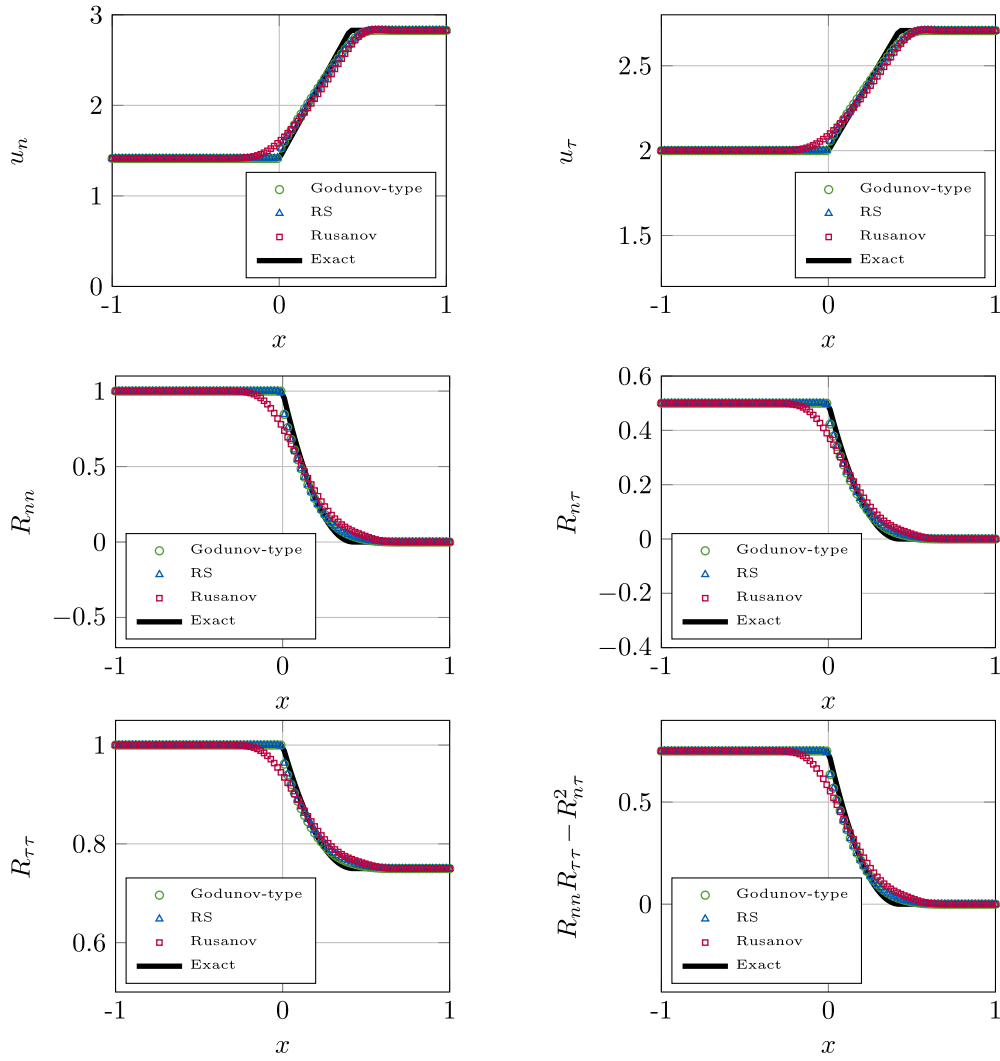


FIGURE E.1. Case 7 numerical solutions with  $N_c = 100$ ,  $t_f = 0.15 \frac{\mathcal{L}}{\sqrt{R_{nn}^L}}$ .

APPENDIX F. MESH SCHEMES

In the non-conservative hyperbolic system framework, there may be unique jump relations when non-conservative terms are not active in the GNL fields (see for instance [1] two-phase flow models). However when the non-conservative terms are active in the GNL fields, no unique jump relations are available as in the model considered in this paper. In this framework where the uniqueness of jump relations is not established, different types of Finite Volume methods may be considered.

Let us consider the following hyperbolic non-conservative system:

$$\partial_t \mathbf{w} + \mathcal{A}(\mathbf{w}) \partial_n \mathbf{w} = 0. \tag{F.1}$$

Let us consider the linear path  $\chi$  also used to obtain the approximate shock relations (2.7):

$$\chi(s, \mathbf{w}^l, \mathbf{w}^r) = \mathbf{w}^l + s(\mathbf{w}^r - \mathbf{w}^l), \quad s \in [0, 1]. \tag{F.2}$$

The formal integration of  $\mathcal{A}(\chi(s, \mathbf{w}^l, \mathbf{w}^r)) \partial_s \chi(s, \mathbf{w}^l, \mathbf{w}^r)$  on  $[0, 1]$  can be used to construct numerical non-conservative mesh schemes (see [13, 26], and also [3] for a more general framework).

- Several linear path mesh schemes have been proposed in the literature to handle non-conservative hyperbolic systems (see [2, 6, 14, 18, 35, 39]).
- One may also refer to Parés [33], Muñoz-Ruiz and Parés [29], Chalons and Coquel [8], Chalons [7] for in-cell reconstruction schemes. The Parés-like mesh scheme is an extension of the Godunov scheme to the non-conservative framework assuming approximate jump conditions.

Similarly to the basic idea of the Godunov scheme introduced in the conservative framework, the solution of the exact Riemann problem is averaged to piecewise constant states to give state at time  $t^{N+1}$  under a CFL condition  $1/2$ , as follows:

$$\begin{aligned} \mathbf{w}_i^{N+1} = & \frac{1}{\delta x} \left( \int_{x_{i-1/2}}^{x_i} \tilde{\mathbf{w}} \left( \frac{x - x_{i-1/2}}{\delta t^N}; \mathbf{w}_{i-1}^N, \mathbf{w}_i^N \right) dx \right. \\ & \left. + \int_{x_i}^{x_{i+1/2}} \tilde{\mathbf{w}} \left( \frac{x - x_{i+1/2}}{\delta t^N}; \mathbf{w}_i^N, \mathbf{w}_{i+1}^N \right) dx \right). \end{aligned} \tag{F.3}$$

The projected solution appearing in (F.3) inherits the positivity properties for the projected quantities. Mesh scheme (F.3) can rewrite:

$$\frac{\mathbf{w}_i^{N+1} - \mathbf{w}_i^N}{\delta t^N} + \frac{1}{\delta x} \left( \mathbf{D}_{i-1/2}^+ + \mathbf{D}_{i+1/2}^- \right) = 0, \tag{F.4}$$

where:

$$\mathbf{D}_{i+1/2}^- = - \int_{-\infty}^0 \left( \tilde{\mathbf{w}}(v; \mathbf{w}_i^N, \mathbf{w}_{i+1}^N) - \mathbf{w}_i^N \right) dv, \tag{F.5}$$

$$\mathbf{D}_{i-1/2}^+ = - \int_0^{\infty} \left( \tilde{\mathbf{w}}(v; \mathbf{w}_{i-1}^N, \mathbf{w}_i^N) - \mathbf{w}_i^N \right) dv. \tag{F.6}$$

It has been shown in [29] Section 4, that the sum  $\mathbf{D}_{i-1/2}^+ + \mathbf{D}_{i+1/2}^-$  rewrites:

$$\begin{aligned} \mathbf{D}_{i-1/2}^+ + \mathbf{D}_{i+1/2}^- = & \int_0^1 \mathcal{A}(\chi(s, \mathbf{w}_{i-1/2}, \mathbf{w}_i)) \partial_s \chi(s, \mathbf{w}_{i-1/2}, \mathbf{w}_i) ds \\ & + \int_0^1 \mathcal{A}(\chi(s, \mathbf{w}_i, \mathbf{w}_{i+1/2})) \partial_s \chi(s, \mathbf{w}_i, \mathbf{w}_{i+1/2}) ds. \end{aligned} \tag{F.7}$$

In the case of a linear path  $\chi$  and a convection matrix  $\mathcal{A}(\mathbf{w})$  linear with respect to  $\mathbf{w}$  (which is the case of the matrix defined in (F.11)):

$$\begin{aligned} \int_0^1 \mathcal{A}(\chi(s, \mathbf{w}^l, \mathbf{w}^r)) \partial_s \chi(s, \mathbf{w}^l, \mathbf{w}^r) ds = & \mathcal{A} \left( \int_0^1 \chi(s, \mathbf{w}^l, \mathbf{w}^r) ds \right) (\mathbf{w}^r - \mathbf{w}^l) \\ = & \mathcal{A} \left( \frac{\mathbf{w}^r + \mathbf{w}^l}{2} \right) (\mathbf{w}^r - \mathbf{w}^l). \end{aligned} \tag{F.8}$$

This leads to:

$$\begin{aligned} \mathbf{D}_{i-1/2}^+ + \mathbf{D}_{i+1/2}^- = & \mathcal{A} \left( \frac{\mathbf{w}_{i-1/2} + \mathbf{w}_i}{2} \right) (\mathbf{w}_i - \mathbf{w}_{i-1/2}) \\ & + \mathcal{A} \left( \frac{\mathbf{w}_i + \mathbf{w}_{i+1/2}}{2} \right) (\mathbf{w}_{i+1/2} - \mathbf{w}_i). \end{aligned} \tag{F.9}$$

- The mesh scheme (4.23) used in the paper is similar to the mesh schemes used by Forestier *et al.* [18] and Berthon *et al.* [2] in a turbulent flow framework (respectively  $k - \epsilon$  compressible turbulence model and a compressible second-order turbulence model) where non-conservative products also occur in the GNL fields, leading to the use of approximate jump relations as in this paper.

We consider the following unknown:

$$\mathbf{w} = (u_n, R_{nn}, u_\tau, R_{n\tau}, R_{\tau\tau}). \tag{F.10}$$

Let  $\mathcal{A}$  be the convective matrix of system (2.2).

$$\mathcal{A} = \begin{pmatrix} u_n & 1 & 0 & 0 & 0 \\ 2R_{nn} & u_n & 0 & 0 & 0 \\ 0 & 0 & u_n & 1 & 0 \\ R_{n\tau} & 0 & R_{nn} & u_n & 0 \\ 0 & 0 & 2R_{n\tau} & 0 & u_n \end{pmatrix}. \tag{F.11}$$

The mesh scheme (4.23) may be rewritten:

$$\frac{\mathbf{w}_i^{N+1} - \mathbf{w}_i^N}{\delta t^N} + \frac{1}{\delta x} \mathcal{A} \left( \frac{\mathbf{w}_{i-1/2} + \mathbf{w}_{i+1/2}}{2} \right) (\mathbf{w}_{i+1/2} - \mathbf{w}_{i-1/2}) = 0. \tag{F.12}$$